Atmospheric Energetics over the Tropical Pacific during the ENSO Cycle

DI DONG

State Key Laboratory of Numerical Modeling for Atmospheric Sciences and Geophysical Fluid Dynamics, Institute of Atmospheric Physics, Chinese Academy of Sciences, and College of Earth Science, University of Chinese Academy of Sciences, Beijing, China

JIANPING LI

State Key Laboratory of Earth Surface Processes and Resource Ecology, and College of Global Change and Earth System Science, Beijing Normal University, and Joint Center for Global Change Studies, Beijing, China

LIDOU HUYAN AND JIAQING XUE

State Key Laboratory of Numerical Modeling for Atmospheric Sciences and Geophysical Fluid Dynamics, Institute of Atmospheric Physics, Chinese Academy of Sciences, and College of Earth Science, University of Chinese Academy of Sciences, Beijing, China

(Manuscript received 29 June 2016, in final form 21 January 2017)

ABSTRACT

The atmospheric perturbation potential energy (PPE) over the tropical Pacific is calculated and analyzed in a composite ENSO cycle. The PPE over the tropical Pacific troposphere increases during El Niño and decreases during La Niña, displaying two centers symmetrical about the equator and delaying the central–eastern Pacific SST anomaly by two months. Generated from atmospheric diabatic heating, the smaller part of PPE in the lower troposphere varies synchronously with the central–eastern Pacific SST through sensible heating, while the larger part of PPE lies in the mid- and upper troposphere and lags the central–eastern Pacific SST about one season because of latent heat release. As the tropical Pacific PPE peaks during the boreal late winter in an El Niño event, two anticyclones form in the upper troposphere as a result of the Gill model response. More PPE is converted to atmospheric kinetic energy (KE) above the central–western Pacific, but less over the eastern Pacific, leading to intensified Hadley circulations over the central–western Pacific and weakened Hadley circulations over the eastern Pacific. The strengthened Hadley circulations cause surface easterly wind bursts through KE convergence in the western equatorial Pacific, which may trigger a La Niña event. The reverse situation occurs during La Niña. Thus, the response of the Hadley circulations in the central–western Pacific provides a negative feedback during the ENSO cycle.

1. Introduction

El Niño–Southern Oscillation (ENSO) is a dominant mode of ocean–atmosphere interaction in the tropical Pacific Ocean on an interannual time scale. Although numerous studies have investigated this phenomenon (e.g., Neelin et al. 1998, and references therein), few have paid attention to the oceanic and atmospheric energetics during El Niño or La Niña. Since the twenty-first century, studies of ENSO energetics have provided a new perspective to help understand ENSO dynamics. Goddard and Philander (2000) pioneered the research on the oceanic energetics of El Niño and La Niña and found that sea surface winds work against ocean pressure gradients and generate buoyancy power; this is responsible for the change of oceanic gravitational available potential energy (Oort et al. 1989), which dominates the anomalous energy of the tropical Pacific Ocean interannually. They also point out that the ocean gains energy as the air–sea system evolves from El Niño to La Niña and loses energy as La Niña changes to El Niño. More recently, oceanic energetics have been further investigated in terms of the predictability (Fedorov et al. 2003), stability (Philander and Fedorov 2003; Fedorov 2007), energy budget (Brown and Fedorov 2008, 2010), and diversity (Hu et al. 2014) of ENSO events.

Corresponding author e-mail: Prof. Jianping Li, ljp@bnu.edu.cn

DOI: 10.1175/JCLI-D-16-0480.1

Previous studies of ENSO energetics mainly focused on the tropical Pacific Ocean for its large inertia, but there are few studies on the atmospheric energetics, even though the ENSO signal is also strong in the tropical Pacific atmosphere. Li et al. (2011) found that, during El Niño or La Niña, sea surface temperature anomalies (SSTa) can influence the tropical and even global atmospheric energies, leading to anomalous atmospheric circulations. Thus, atmospheric energetic responses deserve careful investigations to better understand how the tropical SST forces the atmosphere. According to Lorenz (1955), there is only a small percent of total potential energy, defined as atmospheric available potential energy [APE; APE in this paper refers particularly to the available potential energy defined by Lorenz (1955)], available for conversion to kinetic energy (KE) to change the air motions; thus, APE plays a major part in atmospheric energetics. Since APE is computed on a global average, it is not a powerful tool to investigate the local atmospheric energetics. Li and Gao (2006) proposed the atmospheric perturbation potential energy (PPE) theory to extend APE to a regional scale. Wang et al. (2015) found that the tropical atmospheric PPE has a high partial correlation with ENSO when the KE component is removed, but the relationship between KE and ENSO is weakened when removing the PPE signal. This indicates that PPE acts as a bridge to link the Pacific Ocean and the atmospheric circulations during ENSO. Thus, analyzing the energetic transport and conversion processes of the topical Pacific atmosphere is an essential part to understand the energy cycle of the tropical Pacific air–sea system in ENSO events.

The anomalous atmospheric events that trigger El Niño (La Niña) usually occur in the boreal spring, but the events that result in the onset of El Niño and La Niña remain debated (Lengaigne et al. 2004). One of the most common hypotheses is the impact of intraseasonal wind activities over the western Pacific, often referred as westerly wind bursts (WWBs). Observational analysis (McPhaden et al. 1988; Vecchi and Harrison 2000; Harrison and Chiodi 2009), case studies (Chen et al. 2015; Hu and Fedorov 2016), linear theory (Godfrey 1975; McCreary 1976; Moore and Philander 1977), and numerical modeling (Giese and Harrison 1990, 1991; Boulanger et al. 2001; Belamari et al. 2003, Lopez et al. 2013) have described the mechanisms of how wind variability in the western and central tropical Pacific can drive SSTa in the central and eastern equatorial Pacific. WWBs are usually considered external and part of a stochastic forcing because of their short time scales, but some studies have suggested that the occurrence and characteristics of WWBs depend to some extent on the state of ENSO components (McPhaden and Yu 1999; Vecchi and Harrison 2000; Yu et al. 2003; Eisenman et al. 2005; Lopez et al. 2013). The oscillatory nature of ENSO requires both positive (Bjerknes 1969) and negative (e.g., Suarez and Schopf 1988; Jin 1997a,b; Picaut et al. 1997; Weisberg and Wang 1997) ocean–atmosphere feedbacks. Since the westerly wind bursts are possibly a triggering mechanism for El Niño, and easterly wind bursts for La Niña, it is essential for ENSO feedback mechanisms to explain how the increased SST in the central–eastern Pacific during El Niño can result in easterly wind bursts in the western Pacific that trigger a La Niña event. In this study, the atmospheric energy transport and conversion processes over the tropical Pacific are explored based on two reanalysis datasets, and the regional Hadley circulations over the central–western Pacific are found to play an important role in ENSO negative feedback as a result of its close link with the western Pacific surface zonal winds. It aims to deepen our understanding of tropical air–sea interactions and mechanisms of negative feedback in the ENSO cycle.

2. Theories and data

a. *Atmospheric PPE*

Margules (1910) proposed the atmospheric energy availability first, but the concept of APE had not been widely accepted until Lorenz (1955) formulated the modern framework of atmospheric energetics. Although APE helps diagnose the global atmosphere energy budget (e.g., Oort 1964, 1971; Peixóto and Oort 1974), it is not a powerful tool in analyzing regional atmospheric energetics, because it is computed on a global average. Therefore, several improvements have been made to expand Lorenz's APE theory to a local sale (e.g., Smith 1969; Johnson 1970; Smith et al. 1977; Edmon 1978). Although these studies added the boundary energy fluxes, they still adopted the original APE formulation, which is not suitable to investigate the local atmospheric energetics. Furthermore, APE defines the minimum total potential energy (TPE) as the atmospheric reference state when the stratification is horizontal and statically stable; however, this reference condition is ideal and physically unreachable. Because of these limitations, Gao et al. (2006) defined the conditional minimum TPE as the reference state, as they found that the atmosphere is under physical constraints during the adiabatic redistribution. To formulate local APE, Li and Gao (2006) proposed the PPE as the difference in

atmospheric TPE between the actual state and the conditional minimum reference state via adiabatic redistribution:

$$\mathrm{PPE} = P - \overline{P} = \frac{1}{(1+\kappa)\gamma_d p_{00}^{\kappa}} \int_{\theta_s}^{\theta_T} (p^{1+\kappa} - \overline{p}^{1+\kappa})\, d\theta, \quad (1)$$

where P is the actual total potential energy and p is pressure; variables at the conditional minimum reference state are denoted with an overbar; p_{00} is the reference pressure (usually taken as 1000 hPa); $\kappa = R/c_p$, where R is the gas constant of dry air, and c_p is the specific heat at constant pressure; $\gamma_d = g/c_p$ is the dry adiabatic lapse rate; and θ is potential temperature. We can expand P in series and write the PPE equation in isobaric coordinates (detailed derivations can be found in the appendixes):

$$\mathrm{PPE} = \sum_{i=1}^{\infty} \mathrm{PPE}_i = \sum_{i=1}^{\infty} \frac{p_{00}^{(i-1)\kappa} \prod_{j=0}^{i-1} (1+\kappa-j)}{i!\gamma_d(1+\kappa)} \int_0^{p_S} \frac{T'^i}{p^{(i-1)(1+\kappa)}} \left(-\frac{\partial\overline{\theta}}{\partial p}\right)^{-i+1} dp, \quad (2)$$

where PPE_i is the ith-moment term of PPE; T' is the perturbation temperature from the reference state; and p_s is the surface pressure. The local TPE deviated from the global reference state is represented by PPE, which reflects the perturbation of local atmospheric isentropics from their global mean position. According to Li and Gao (2006), PPE_1 is the dominant part of PPE in the regional scale, which has not been analyzed in the previous studies. The higher-moment terms of PPE depend on both perturbation temperature and vertical gradient of mean potential temperature, but they are much smaller compared with PPE_1 locally.

The governing equations of PPE_1 and atmospheric KE are

$$\frac{1}{g}\int_0^{p_s} \frac{\partial \mathrm{PPE}_1}{\partial t}\, dp = C_k + G - \mathrm{HBF}_{\mathrm{PPE}} \quad \text{and} \quad (3)$$

$$\frac{1}{g}\int_0^{p_s} \frac{\partial \mathrm{KE}}{\partial t}\, dp = -C_k + D - \mathrm{HBF}_{\mathrm{KE}}, \quad (4)$$

where C_k represents the energy conversion between PPE_1 and KE: when $C_k < 0$, PPE_1 is converted to KE, and, when $C_k > 0$, KE is converted to PPE_1; G represents the diabatic heating to the atmosphere; and D stands for viscous dissipation. The HBF terms are the horizontal boundary fluxes. The governing equations show that the atmospheric adiabatic heating G first changes PPE but cannot change KE directly; thus, it is the energy conversion process C_k that serves as a bridge to link the diabatic heating with the atmosphere circulation change.

Therefore, the concept of PPE differs from the APE mainly in two aspects: one is that it redefines the reference state as the conditional minimum energy state through atmospheric adiabatic regulation under physical and mathematical constraints; the other is that PPE retains the first-moment term PPE_1, which is the dominant part in the local scale. More details on the derivation of PPE and related governing equations can be found in the appendixes and the supplementary materials in Wang et al. (2015). Several studies (Gao and Li 2012, 2013; Wang et al. 2012, 2015; Li et al. 2016) have shown that PPE can serve as a powerful tool in exploring regional atmospheric energetics.

b. Data and method

Two datasets have been used for comparison: one is the NCEP Reanalysis-2 (NCEP-2; Kanamitsu et al. 2002) data provided by the NOAA/OAR/ESRL Physical Sciences Division (PSD), Boulder, Colorado, from their website (https://www.esrl.noaa.gov/psd/data/gridded/data.ncep.reanalysis2.html), and the second is the monthly European Centre for Medium-Range Weather Forecasts (ECMWF) interim reanalysis (ERA-Interim; Dee et al. 2011). The period is from 1979 to 2015; the horizontal grid resolution of both datasets is 2.5° × 2.5°, because this study mainly focuses on the large-scale atmospheric energetics. In the vertical, 11 levels (1000–150 hPa) are selected to cover the whole troposphere. In addition, sensible and latent heat flux and precipitation rate data from NCEP-2 are also used to analyze the diabatic heating. SST data are from the Met Office Hadley Centre (Rayner et al. 2003).

PPE is calculated as the sum of PPE_1 and PPE_2, because the higher-moment terms of PPE are much smaller and negligible. The Niño-3.4 index from the Climate Prediction Center of the National Oceanic and Atmospheric Administration (NOAA) is used to identify El Niño and La Niña events. Composite analysis and lead–lag correlation methods are adopted to analyze the atmospheric energetic features. Since we want to see how atmospheric and oceanic energies change during the ENSO cycle, only ENSO events that contain an El Niño–La Niña phase shift have been selected and

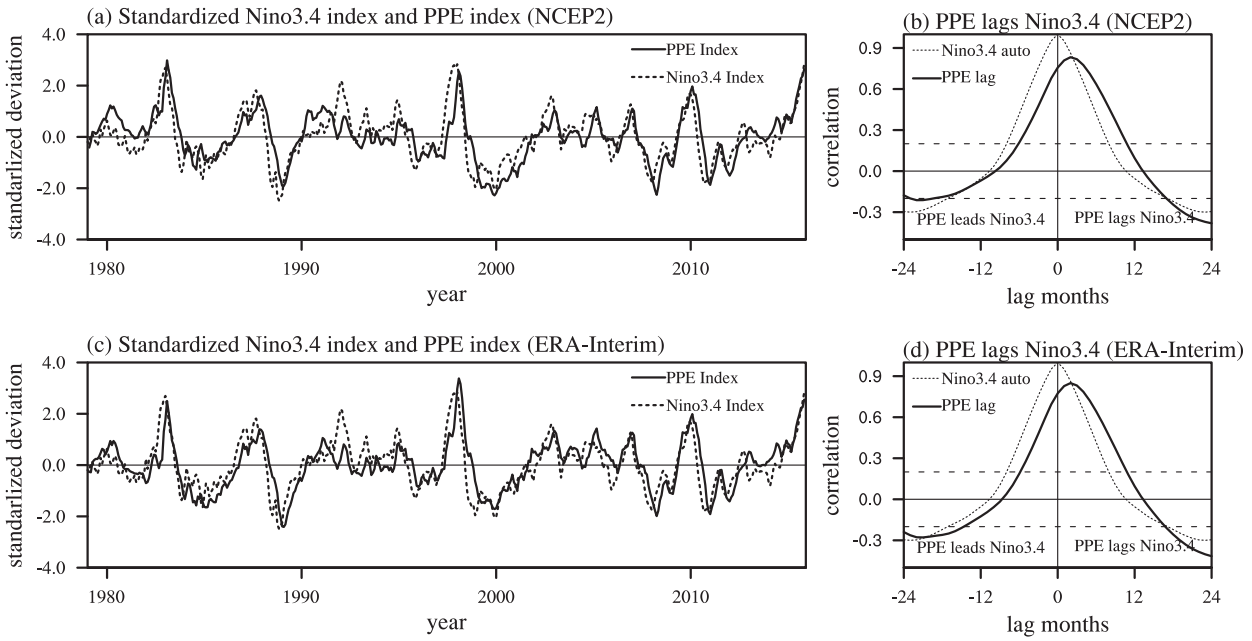

FIG. 1. (a) Standardized time series of the Niño-3.4 index (dotted line) and the PPE index (solid line) based on NCEP-2 data. (b) The lead–lag correlation between Niño-3.4 and the PPE index with NCEP-2 data (solid line). Positive values indicate that PPE lags Niño-3.4. The dotted line is the autocorrelation of the Niño-3.4 index; dashed lines show the 95% confidence level (the Student's *t* test). (c),(d) As in (a),(b), but using ERA-Interim data.

composited (1982–84, 1987–89, 1994–96, 1997–99, 2004–06, 2006–08, and 2009–11).

3. PPE variation in the tropical Pacific during the ENSO cycle

a. Temporal variability of PPE

The Niño-3.4 index is defined as the areal average of SSTa in the central–eastern equatorial Pacific, reflecting the intensity of anomalous oceanic warming or cooling therein. Similarly, the areal average of the tropospheric PPE anomaly (PPEa) over the tropical Pacific (30°S–30°N, 150°E–90°W) is defined as the PPE index. Standardized time series of PPE and Niño-3.4 indices are shown in Figs. 1a,c. Meanwhile, the lead–lag correlations of the two indices are given in Figs. 1b,d.

The PPE index shows a positive correlation, remarkable from both datasets, with the Niño-3.4 index interannually. This demonstrates that the tropospheric atmosphere over the tropical Pacific gains more energy in El Niño when the central–eastern Pacific is warmer, while during La Niña, when the central–eastern Pacific Ocean is colder, less energy is transported from the sea to the air. The high correspondence indicates a strong air–sea coupling effect during ENSO events.

Furthermore, the PPE index does not change synchronously with the Niño-3.4 index, which is more clearly demonstrated in the lead–lag correlations in Fig. 1b,d: The PPE index lags the Niño-3.4 index about 2 months in both two datasets, showing that the tropical Pacific atmosphere has a delayed response to the central–eastern Pacific SST heating or cooling. When an El Niño event reaches its mature phase in December, the PPE over the tropical Pacific continues increasing and peaks in February of the next year. Such delayed atmospheric response has been previously noticed and confirmed (Angell 1981; Pan and Oort 1983; Reid et al. 1989; Kumar and Hoerling 2003; Su et al. 2005; Li et al. 2011). The lagged response demonstrates that energy is initially stored in the tropical Pacific Ocean and then released to the atmosphere above. Since the atmosphere reacts to the diabatic heating quickly, the 2-month lag indicates that, although SST reaches its maximum in December, the diabatic heating to the atmosphere is not in pace with SSTa but lags it by about 2 months.

b. Spatial variation of PPE

The seasonal mean SSTa and the tropospheric PPEa in the tropical Pacific region are shown in Figs. 2 and 3 in a composite ENSO cycle. Here, we define the El Niño developing year as year −1, the El Niño decaying and La

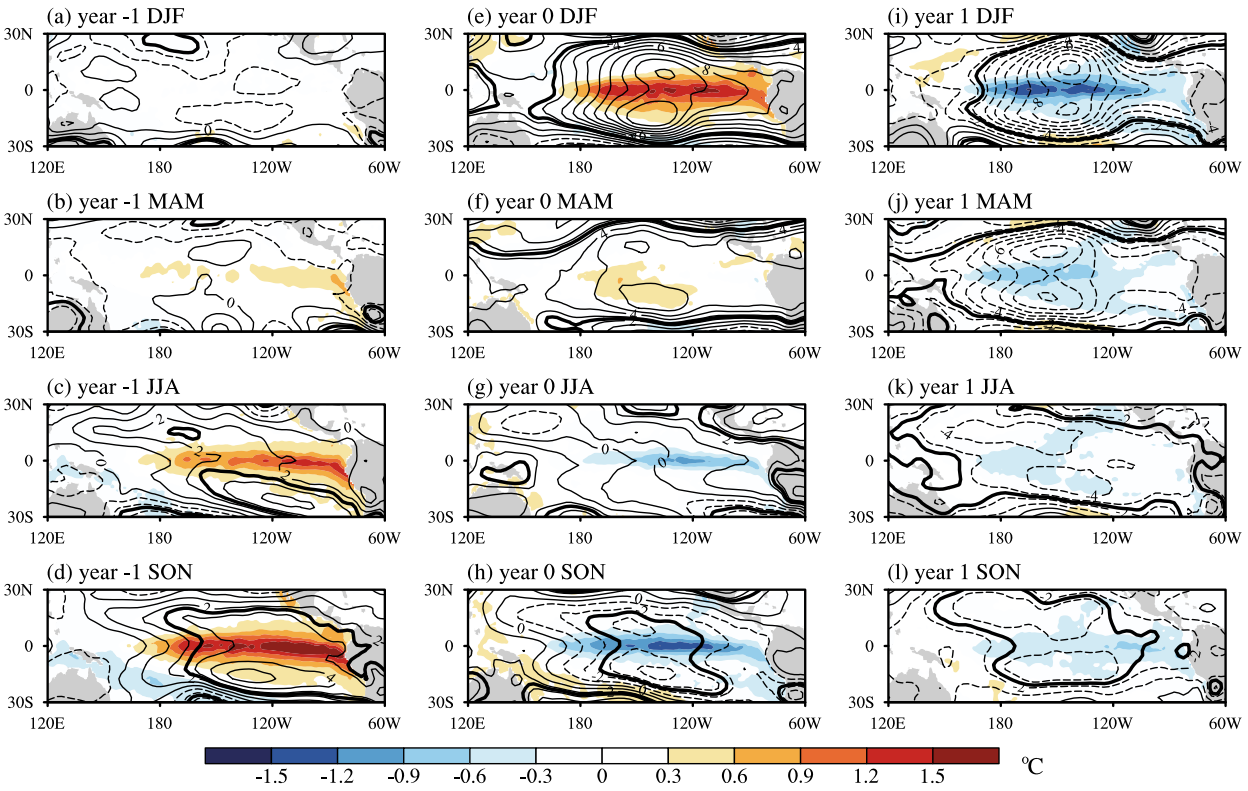

FIG. 2. Seasonal evolution of SSTa and PPEa in a composite ENSO cycle based on NCEP-2 data. Color shading is composite seasonal SSTa (°C); contour lines are seasonal tropospheric PPEa (10^6 J m^{-2}; negative values are indicated by dashed contours; areas within the thick contours are significant at the 95% confidence level).

Niña developing year as year 0, and the La Niña decaying year as year 1. In spite of some discrepancies, the PPEa spatial patterns from the two datasets are quite similar. In the boreal summer and autumn of year −1, as the central–eastern Pacific SST rises, the PPE over the tropical Pacific increases as well and displays two maximum centers with its southern part stronger. In the boreal winter of year 0, when El Niño reaches its peak phase, the anomalous PPE shows two maximum centers, lying symmetrically about the equator between 150° and 120°W. This two-center distribution is consistent with the Gill (1980) model response to the tropical atmospheric diabatic heating. The heating center in the Gill model is around 5 km in the tropical atmosphere rather than in the air–sea interface, indicating that the heating center to PPE lies in the midtroposphere. In MAM of year 0, El Niño decays quickly and PPE also weakens. In JJA of year 0, the central–eastern Pacific SST becomes anomalously cold, and PPE returns to its normal state. In the following boreal autumn and winter, as La Niña develops and matures, PPEa shows two negative centers on both sides of the equator in the central Pacific Ocean. The process and distribution of PPE variability during La Niña is similar to that in El Niño but in a reverse sign. It is also noted that, although SSTa is mainly confined to the equatorial zone, the PPEa signal extends more widely; this is because air has a much smaller heat content than water and expands more in volume when it absorbs the same amount of heat.

The seasonal evolution shows PPE changes in pace with SST, but the 2-month phase lag is not significant on the seasonal scale. To capture more details of PPE variation during the ENSO cycle, monthly data are analyzed both horizontally and vertically. Figure 4 shows the time–latitude variation of the zonally averaged tropical Pacific PPEa at the lower (Figs. 4b,g), middle (Figs. 4c,h), upper (Figs. 4d,i), and the whole (Figs. 4e,j) troposphere. The time–latitude evolution of the central–eastern Pacific SSTa is also given (Figs. 4a,f). SST changes mainly in the equatorial zone. The peak phase of El Niño and La Niña lies in December, showing a "phase locking" characteristic.

Comparing the variations of PPEa on different layers with SSTa separately, PPEa at the bottom of the troposphere changes consistently with the SSTa. There is no time lag between the two, and they both show their

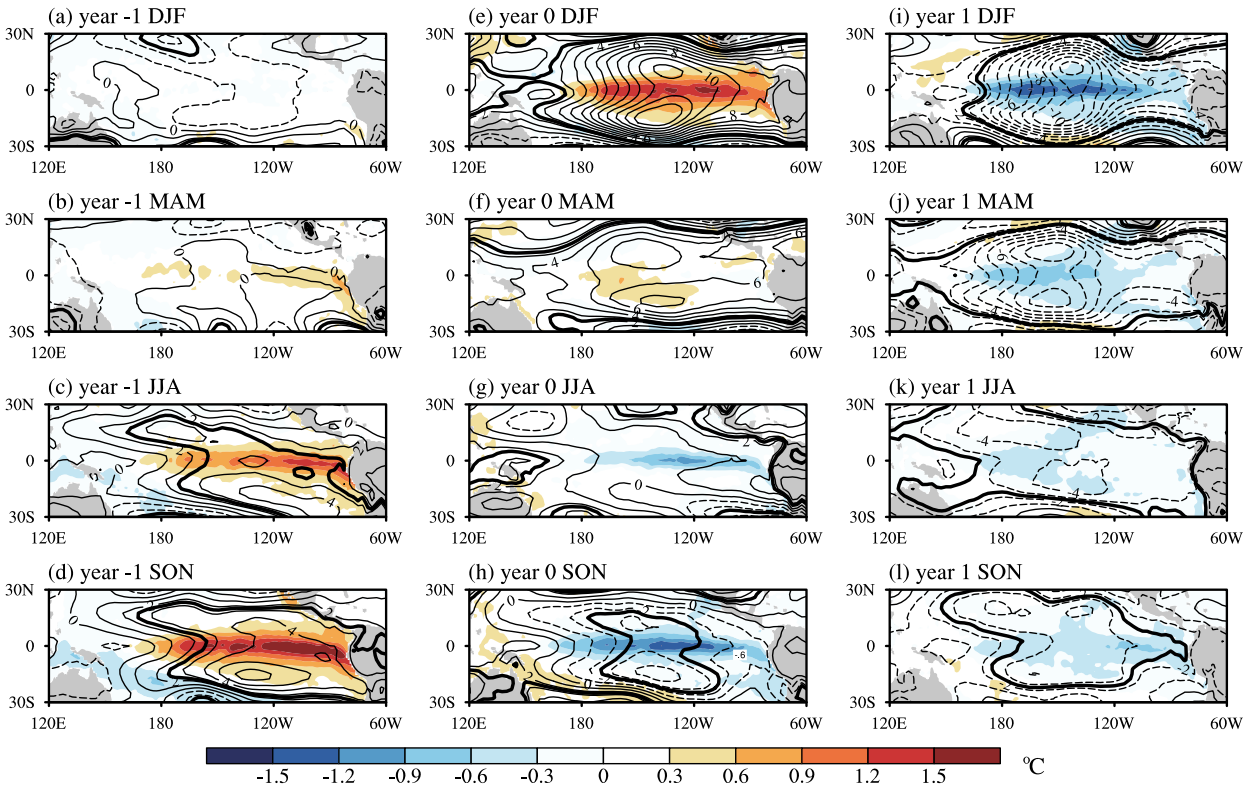

FIG. 3. As in Fig. 2, but using ERA-Interim data.

anomalous centers at the equator. This temporal and spatial consistency indicates the energy change in the low-level troposphere is directly linked to the SST change, and the heat release from the ocean is instant. However, when rising to the midtroposphere (600–300 hPa), PPEa splits into two centers on both sides of the equator and fills the whole tropical Pacific between 30°S–30°N. This reflects that the tropical atmosphere has a larger spatial response scale and is linked to the Gill-type dynamic structure. Compared with the PPEa in the low layers, the PPEa in the midtroposphere is much larger in quantity, demonstrating that the atmosphere gains PPE in El Niño or loses PPE in La Niña, mainly in the midtroposphere. Moreover, the midlayer PPEa has a 2-month lag to the SSTa, which is not found in the bottom layers. In the upper troposphere, the PPEa bears similar features to that in the middle layers but is less significant. The spatial and temporal inconsistency between the SSTa and the mid-to-upper-tropospheric PPEa implies that heating or cooling of the Pacific Ocean influences the mid- and upper-level tropospheric PPEa not in a direct way but through other mechanisms.

The previous analysis shows that the tropical Pacific PPE displays an uneven distribution vertically; the time–height variations of the areal mean tropical Pacific PPEa (30°S–30°N, 150°–90°W) in Fig. 5 illustrate this character more clearly. In the beginning of year −1, PPE becomes anomalously positive at the low layers (1000–700 hPa), and the PPE over 700 hPa is still anomalously small at this time. In the boreal summer of year −1, there exist two PPE positive centers—one below 700 hPa and the other between 300 and 400 hPa—indicating the atmosphere starts to gain energy in the lower and middle troposphere separately during this time. In February of year 0, the PPEa has its maximum center between 500 and 300 hPa, mainly in the midtroposphere. During La Niña, the bottom of the atmosphere loses energy initially, and the midlayer PPE sharply decreases in February of year 1. In addition, the lead–lag correlations between the Niño-3.4 index and the PPE index at different layers in Figs. 5c,d show that there is no time lag in the lower troposphere, but a 2-month lag of PPEa exists in the mid- and upper troposphere.

Therefore, during El Niño and La Niña, the variation of the tropical atmosphere PPE has its strongest part in the middle layer of the troposphere, displaying a Gill model distribution and lagging the central–eastern Pacific SSTa by about 2 months. In the low-level troposphere, the tropical Pacific PPEa bears the same features with the central–eastern Pacific SSTa both in space and

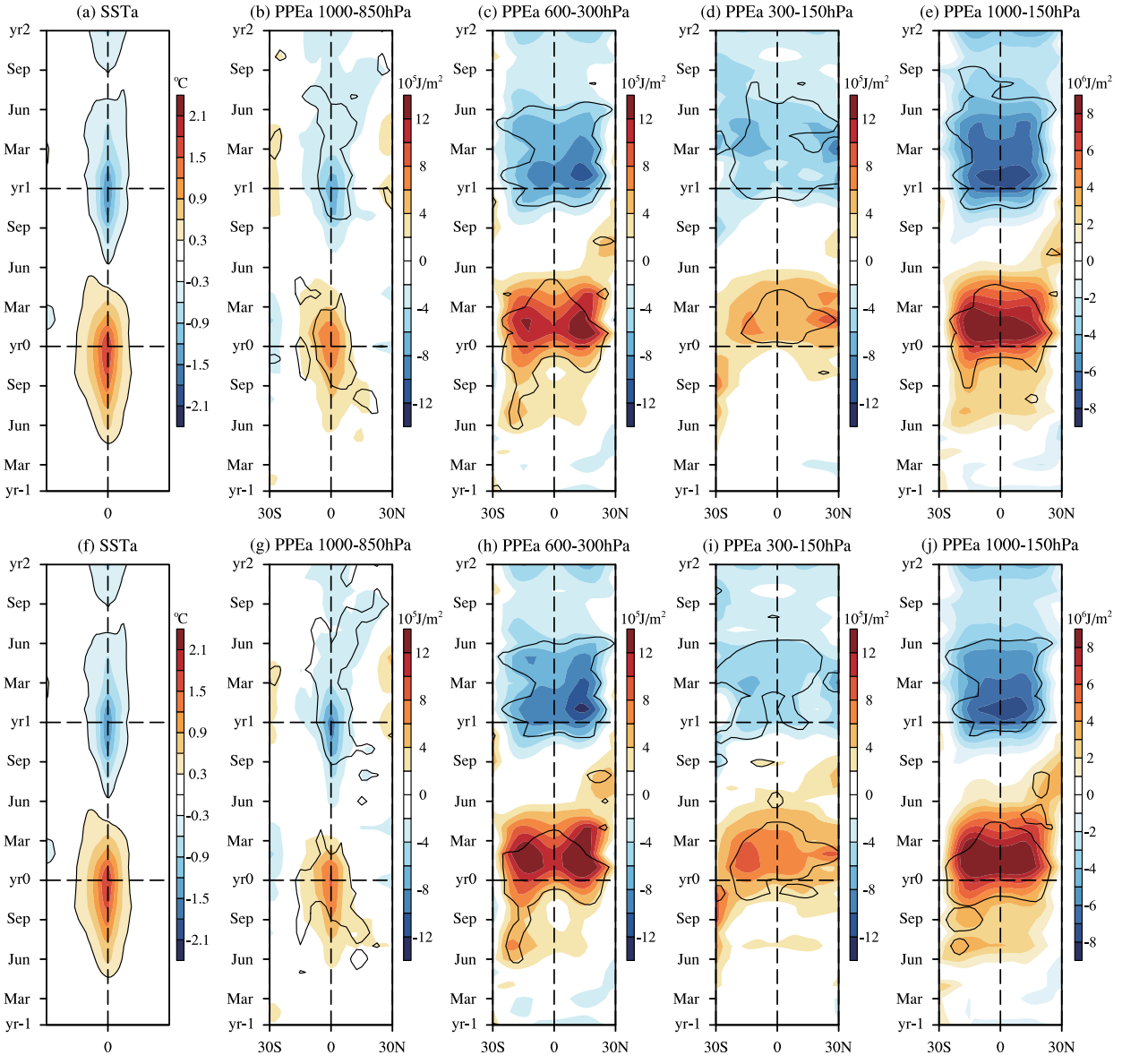

FIG. 4. (a),(f) Composited time–latitude plots of zonally averaged SSTa (°C) of the tropical central–eastern Pacific throughout the composite ENSO cycle. Composited time–latitude variations in zonally averaged PPEa (J m^{-2}) of the tropical Pacific atmosphere (150°–90°W) at the (b) lower (1000–850 hPa), (c) middle (600–300 hPa), (d) upper (300–150 hPa), and (e) the entire troposphere (1000–150 hPa), using NCEP-2 data. Shaded contour intervals are 2×10^5 J m^{-2} in (b)–(d) and 1×10^6 J m^{-2} in (e). (g)–(j) As in (b)–(e), but using ERA-Interim data. Solid contours surround areas that are statistically significant at the 95% confidence level.

time. The uneven PPEa variability in vertical indicates that there are different mechanisms that influence the atmospheric PPE in the lower and middle troposphere.

c. *Diabatic heating to the tropical Pacific atmosphere*

Equation (3) shows that the variation of PPE is influenced by diabatic heating G, energy conversion with KE C_k, and boundary flux HBF. The three terms over the tropical Pacific were calculated and compared (not shown here), and the diabatic heating is the leading term. Besides, C_k and HBF are the inner atmospheric processes that are not linked to SST forcing; thus, we focus on G, because it dominates the PPE variation and reflects how anomalous SST can influence the atmosphere as well.

To investigate the influence of diabatic heating from the Pacific Ocean, sensible heat flux and latent heat release are analyzed. Figure 6 illustrates the time–latitude

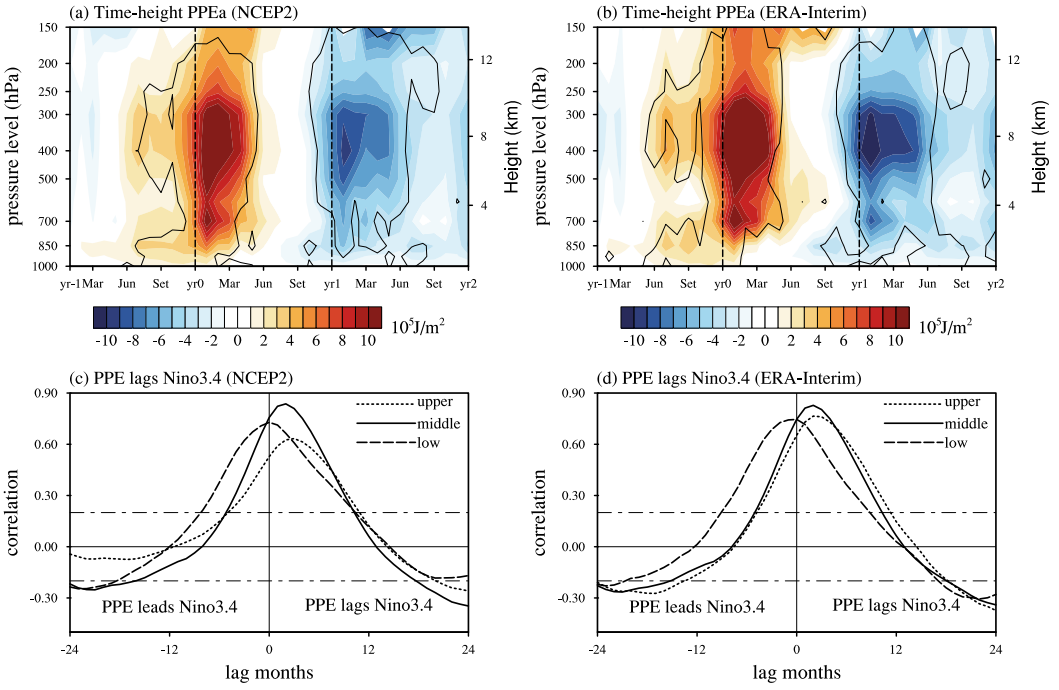

FIG. 5. (a) Time–height plot of mean tropical Pacific PPEa (30°S–30°N, 150°–90°W) throughout the composite ENSO cycle with NCEP-2 data. Shaded contour intervals are 1×10^5 J m^{-2}. Solid contours surround areas that are statistically significant at the 95% confidence level. (c) Lead–lag correlations between the Niño-3.4 index and PPEa at different tropospheric layers [low (dashed), middle (solid), and upper (dotted) layers] based on NCEP-2 data. Positive values mean PPE lags the Niño-3.4 index. (b),(d) As in (a),(c), but with ERA-Interim data.

zonal mean of the temperature difference between the sea and the air (SST $-$ T)—sensible heat flux anomalies in the central–eastern Pacific Ocean. In year -1, as SST becomes warmer, SST $-$ T gets larger, and sensible heat is transported from the Pacific Ocean to the atmosphere. The sensible heat varies consistently with SSTa, and they both reach either a maximum or a minimum in December. Although SSTa can extend 15° in meridional direction, the scope of SST $-$ T is narrower, mainly confined in the equatorial zone; thus, the sensible heating is narrower in meridional direction. Compared with the PPEa at the bottom of the atmosphere, PPEa shows no time lag with sensible heat, but it extends to be wider. This is because air has a small heat content, which expands more in volume when absorbing the same amount of heat, and the heat transport processes in the atmosphere through turbulence and wind advection are also stronger.

Since the atmospheric PPE over the tropical Pacific has its largest part in the middle of the troposphere, which splits into two centers and lags the SSTa by about 2 months, the diabatic heating is expected to be strong in the midtroposphere. Latent heat can only be released in the atmosphere when water vapor condenses; thus, the precipitation rate can serve as proxy data to measure the intensity of latent heat release. Figure 7 shows the time–latitude variations of SSTa, surface latent heat net flux anomaly, precipitation rate anomaly, and the midlevel PPEa in the tropical Pacific region in a composite ENSO cycle. There is increased latent heat flux from the sea in El Niño and decreased latent heat flux in La Niña. Though no time lag exists in the surface latent heat flux anomaly, the 2-month lag is quite significant in precipitation anomalies. Tao et al. (2001) and Schumacher et al. (2004) have found that the latent heating profile in the tropical troposphere contains the maximum stratiform heating in the upper troposphere, the maximum convective heating in the midtroposphere, and the dominant stratiform cooling in the lower troposphere. Besides, they point out that, over the central and eastern Pacific, the monthly mean latent heat profile has its maximum near 8 km; this is also the location of the largest PPE variation center. In temporal variability, the atmospheric latent heating anomaly lags SSTa by about 2 months, because the precipitation rate shows the delayed response. This is in agreement with the time lag of midlevel atmospheric PPEa in Fig. 7d. The time and spatial consistency between the latent heat release and the midlevel PPEa demonstrates the strong diabatic heating or cooling

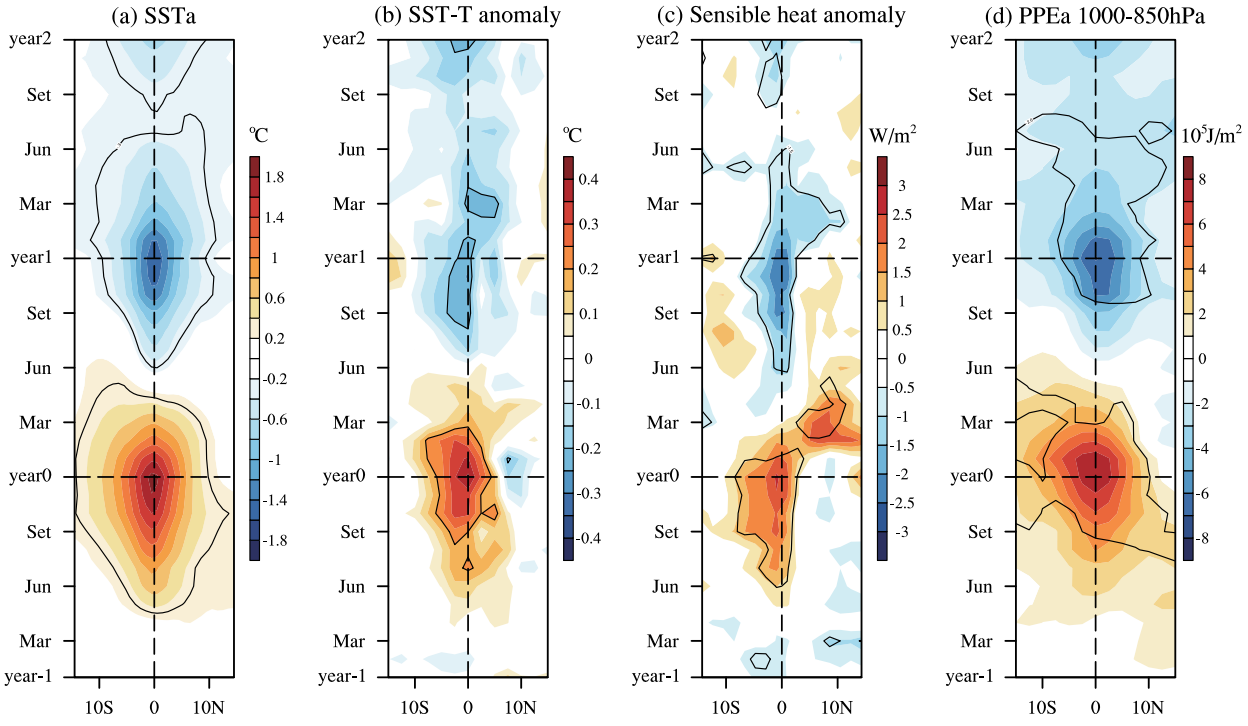

FIG. 6. Time–latitude variations in zonally averaged variables during a composite ENSO cycle: (a) SSTa (°C), (b) anomaly of the temperature difference between sea and air (°C), (c) net sensible heat flux anomaly (W m^{-2}; positive values indicate an upward flux), and (d) PPEa (J m^{-2}) at the bottom of the atmosphere (1000–850 hPa; shaded contour interval is 10^5 J m^{-2}). Solid contours surround areas that are statistically significant at the 95% confidence level.

effect of latent heat release on the midtropospheric PPE in ENSO events.

Thus, the diabatic heating from the ocean influences atmospheric PPE in two aspects: near the sea surface, the atmospheric PPE is directly associated with SSTa through sensible heat exchange; and, in the midtroposphere, the latent heating is the major source of PPE. The delayed response of latent heat release accounts for why the atmospheric PPEa lags the SSTa by about 2 months. This is also reflected in Fig. 5, where there exist two separate centers, one below 700 hPa and the other between 300 and 400 hPa, indicating two heating processes coexist during El Niño development.

4. Energy conversion between PPE and KE

Equations (3) and (4) demonstrate that atmospheric energy can be converted between PPE and KE through C_k, which is defined as

$$C_k = \frac{1}{g}\int_0^{p_s} (\omega\alpha - \overline{\omega\alpha})\, dp, \qquad (5)$$

where ω is the vertical velocity in pressure coordinate, and α is air specific volume. When cold air ascends or warm air descends, C_k is positive and energy is converted from KE to PPE. Conversely, when warm air ascends or cold air descends, C_k is negative, and PPE is converted to KE.

Figure 8 shows the time–longitude variations in tropospheric C_k anomalies (averaged between 10°S and 10°N) during a composite ENSO cycle. The two datasets show similar results: After El Niño matures, C_k reaches its minimum, and more PPE is converted to KE to increase the atmospheric circulation intensity; however, during La Niña, C_k is anomalously positive, and less PPE is converted to KE, weakening the atmospheric motions. The temporal variations between C_k and PPE are consistent and lag SSTa by about 2 months, indicating that atmosphere gains or loses energy from the diabatic heating and changes its circulation through the energy conversion process.

In spite of the PPE anomalous centers lying between 150° and 120°W, C_k shows its maximum or minimum around 180° in the central–western Pacific. Meanwhile, C_k in the easternmost part of the equatorial Pacific exhibits the opposite sign, although it is not quite significant. Figure 9 illustrates this feature more clearly: Figs. 9a,b give the same results on C_k variations over the central–western Pacific in Fig. 8. However, Figs. 9c,d

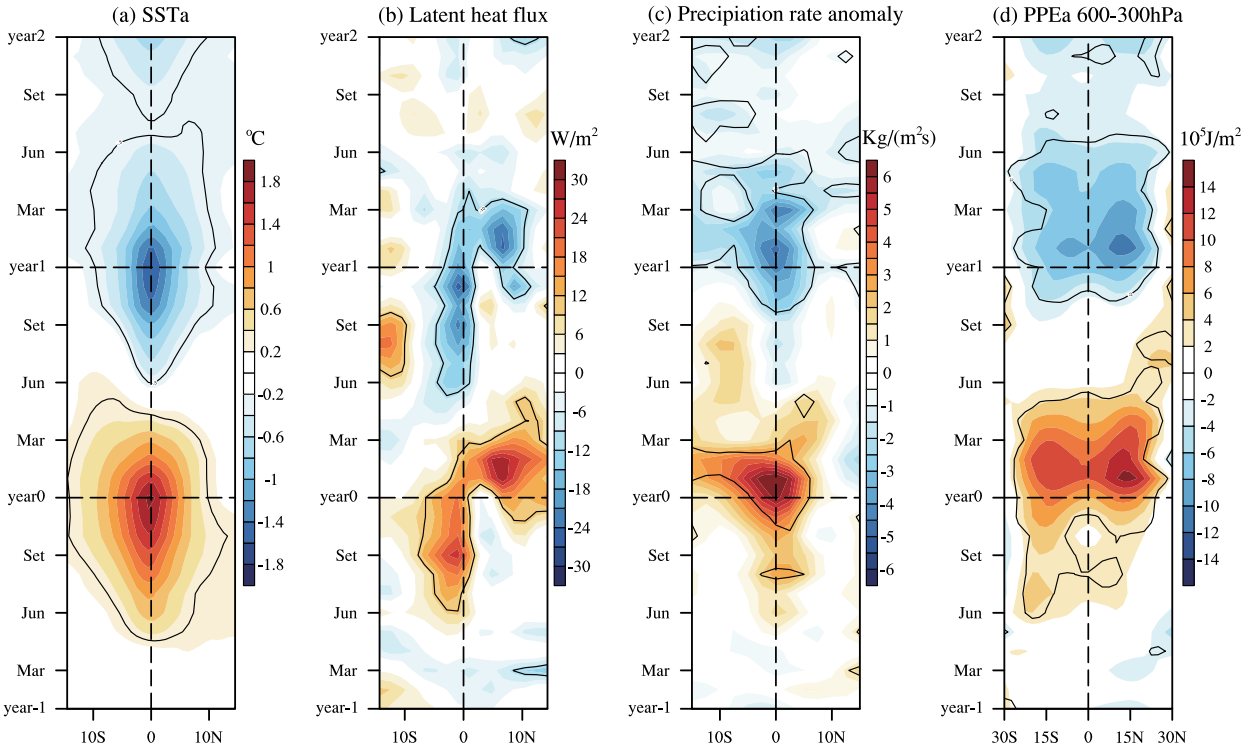

FIG. 7. Time–latitude variations in zonally averaged variables during a composite ENSO cycle. (a) SSTa (°C), (b) net latent heat flux anomaly ($W\,m^{-2}$) from NCEP-2 data, (c) The precipitation rate anomalies ($kg\,m^{-2}\,s^{-1}$), and (d) PPEa ($J\,m^{-2}$) in the midtroposphere (600–300 hPa; shaded contour interval is $10^5\,J\,m^{-2}$). Solid contours surround areas that are statistically significant at the 95% confidence level.

show the C_k anomalies in the eastern Pacific have the opposite signs compared with that in the central–western Pacific, meaning that the atmospheric circulations weaken in El Niño and strengthen in La Niña over the eastern Pacific. The unvarying values of the area-averaged C_k over the two regions in Figs. 9e,f also demonstrates the opposite energy conversion processes.

Thus, the opposite energy conversion processes lie on the east and west of the PPEa centers, indicating that the changed atmospheric PPE has different influences on

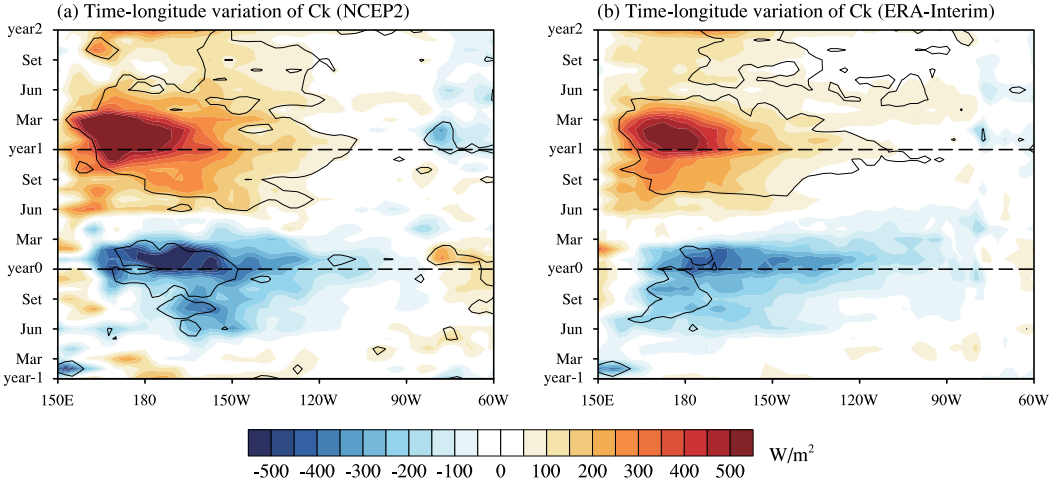

FIG. 8. Time–longitude variations in tropospheric C_k ($W\,m^{-2}$) anomalies during a composite ENSO cycle with (a) NCEP-2 and (b) ERA-Interim data; negative values indicate energy converted from PPE to KE. Solid contours surround areas that are statistically significant at the 95% confidence level.

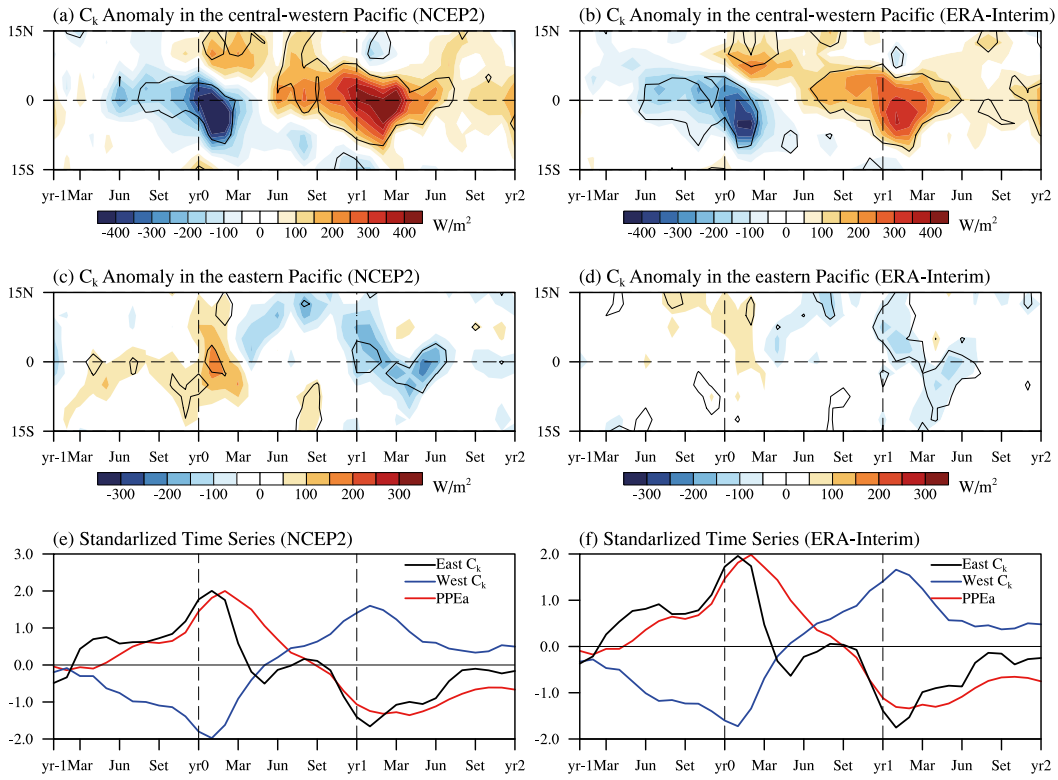

FIG. 9. Time–latitude variations in C_k (W m^{-2}) averaged over the central–western Pacific during a composite ENSO cycle with (a) NCEP-2 and (b) ERA-Interim data. Negative values represent energy converted from PPE to KE. (c),(d) As in (a),(b), but averaged over the eastern equatorial Pacific. (e),(f) Standardized area-averaged PPEa (red), central–western Pacific C_k (blue), and eastern Pacific C_k (black) using both datasets.

the atmospheric circulations over the central–western and eastern Pacific, including the surface wind stresses, which are of great importance in ENSO dynamics.

5. Energetic effects on atmosphere circulations

a. Response of regional Hadley circulations

The remarkable change of PPE and the energy conversion processes are expected to influence the atmosphere circulations over the tropical Pacific in the boreal late winter or early spring after ENSO peaks. It is natural to shed light on the two dominant circulations in the tropics: the Walker circulation and the Hadley circulation. The Walker circulation is an inner part of the air–sea interaction that provides the positive feedback in ENSO dynamics, varying synchronously without any delayed response to the SST. In contrast, the Hadley circulation lags the SST and changes significantly in the decaying phase of ENSO events, which is congruent with PPE and C_k in time (analyzed in the following). This indicates that the Hadley circulation plays an important role in the air–sea interaction after ENSO matures, and we, thus, focus on the regional Hadley circulations and try to explain what effects they may have on the ENSO cycle.

First, we define the Hadley circulation index (HCI) as the difference in the meridional velocities V between the upper troposphere (600–150 hPa) and the lower troposphere (1000–400 hPa). Figures 10 and 11 show how PPEa and the Hadley circulation index evolve during a composite ENSO cycle on a seasonal scale. In the boreal summer and autumn of year −1, PPEa is centered mainly in the southern tropical Pacific, and HCIs in the Southern Hemisphere are negative in the west and positive in the east, meaning that the Hadley circulation over the southwestern Pacific strengthens, and the Hadley cell over the southeastern Pacific weakens. When entering boreal winter, PPEa has two anomalous centers symmetrical about the equator, and the Hadley circulation strengthens in the central–western Pacific and weakens in the east in both hemispheres. This opposite change reflects that opposite energy conversion processes occur on the east and west sides of the PPEa center. During the boreal spring of year 0, a pair of the strengthened Hadley cells in the west remains, but the

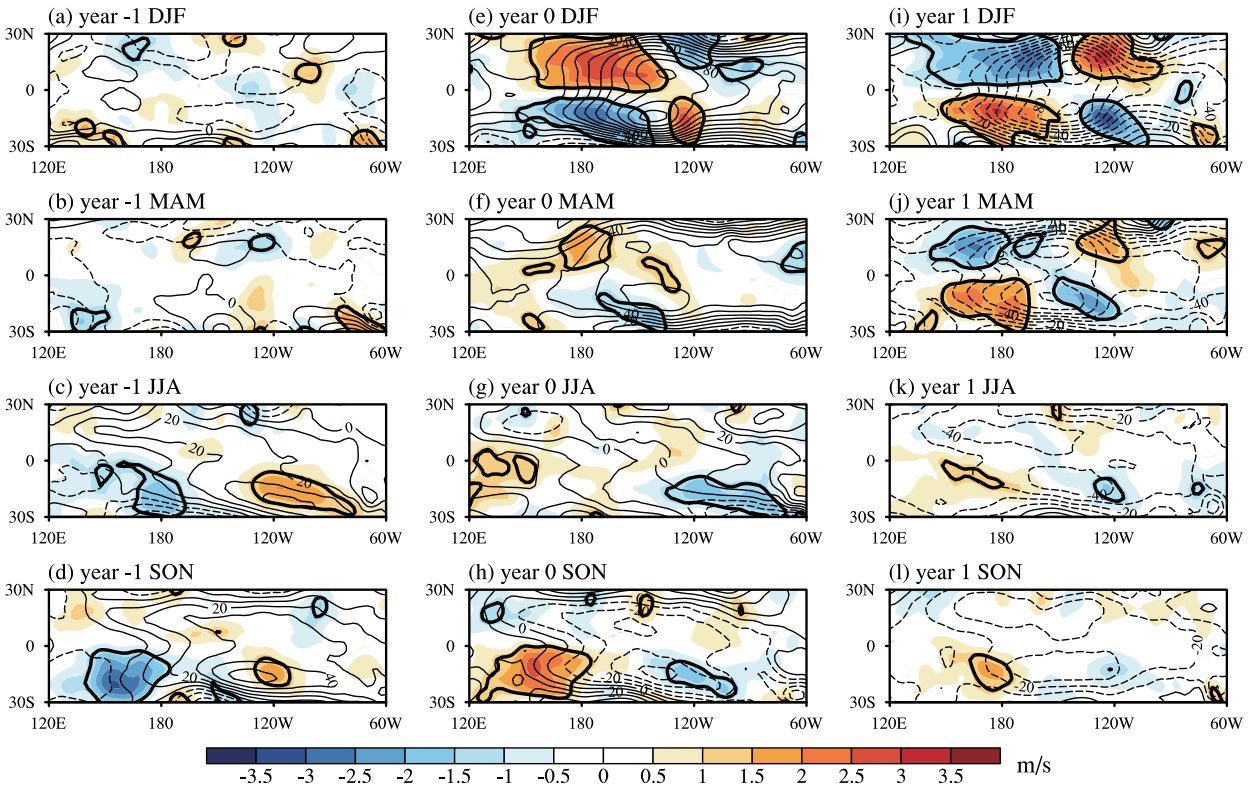

FIG. 10. Shading indicates the seasonal mean of the HCI (defined as $V_{\text{upper}} - V_{\text{lower}}$, see text; areas within thick black contours are significant at the 95% confidence level). Contour lines are PPEa (10^6 J m^{-2}; dashed lines indicate negative values) in a composite ENSO cycle based on NCEP-2 data.

weakened cells in the east disappear. As La Niña develops in year 0 and matures in the boreal winter of year 1, the situation reverses: PPEa has minimum centers around 150°W and the central–western Pacific Hadley circulations weaken in both hemispheres, while the eastern Pacific Hadley cells are stronger.

To see the temporal variations of the regional Hadley circulations, we define the areal mean HCI over the northwestern Pacific (0°–30°N, 150°E–150°W) as the northwest Hadley circulation index (NWHCI) and the areal mean HCI in the northeastern Pacific (0°–30°N, 120°–60°W) as the northeast Hadley circulation index (NEHCI). Similarly, the southwest HCI (SWHCI; 0°–30°S, 150°E–150°W) and southeast HCI (SEHCI; 0°–30°S, 120°–60°W) in the Southern Hemisphere are also defined. The lead–lag correlations between the four indices and the Niño-3.4 index are illustrated in Fig. 12. The results show that the Hadley circulations, in the central–western and eastern Pacific in both hemispheres, have a significant and delayed response to the SST, which is consistent with the lagged responses of PPEa and C_k. When focusing on the western Pacific (Figs. 12a,c), NWHCI and SWHCI have opposite correlations with the Niño-3.4 index, demonstrating that the Northern Hemisphere clockwise Hadley circulations and Southern Hemisphere anticlockwise Hadley circulations in the central–western Pacific both intensify during El Niño and weaken during La Niña. In contrast, for the eastern Pacific, Figs. 12b,d show the Hadley circulations weaken during El Niño and strengthen during La Niña, which is opposite of the western Pacific. Moreover, the linkage between SST and Hadley circulation is stronger in the central–western Pacific, while their correlations are much weaker in the eastern Pacific. This is consistent with the stronger energetic conversion processes over the central–western Pacific in Fig. 8.

The opposite Hadley circulation responses are controlled by both the energetic conversion processes and the Gill-type dynamical structure: After El Niño matures, PPE increases, and two anticyclones form in the upper troposphere as a result of the Gill response. To the west of the PPE center, the southerly winds in the Northern Hemisphere and the northerly winds in the Southern Hemisphere strengthen, and there is wind divergence in the upper troposphere; thus, upward wind

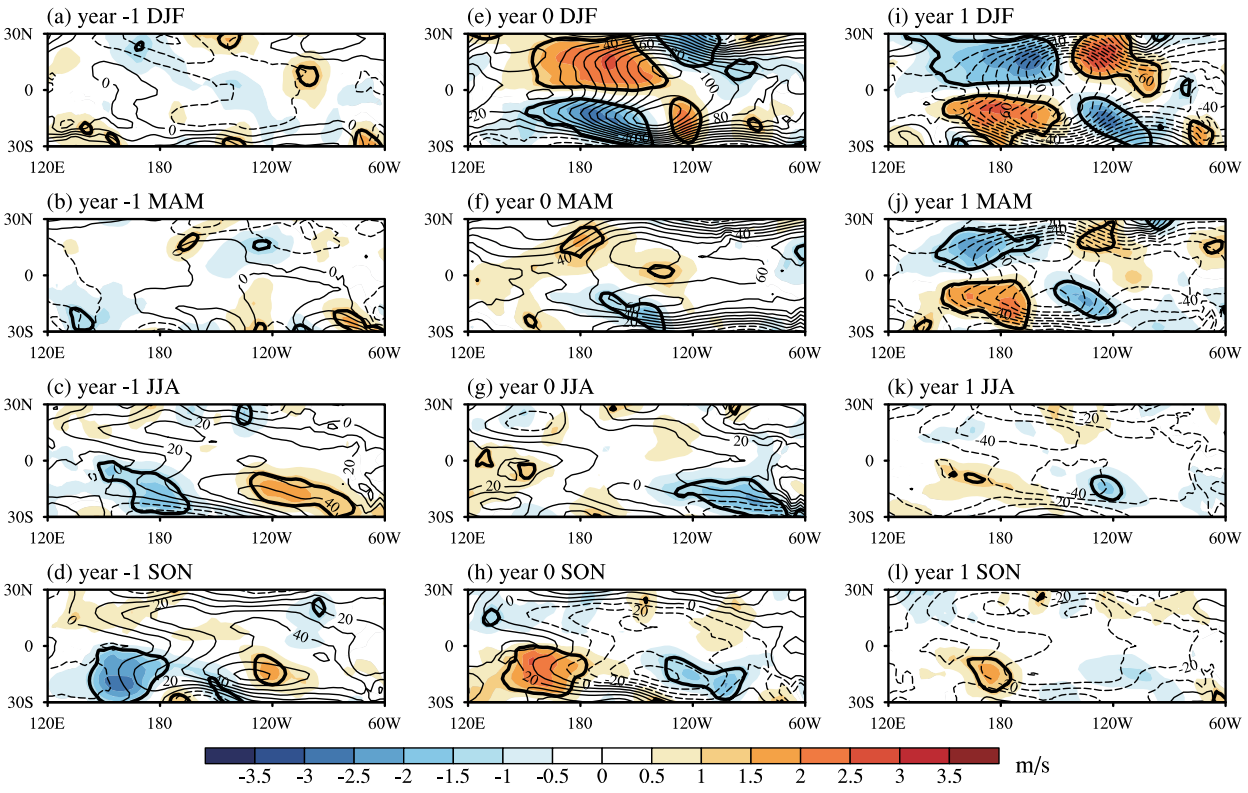

FIG. 11. As in Fig. 10, but using ERA-Interim data.

increases in the central–western Pacific to strengthen the local Hadley circulation. Meanwhile, as warm air rises, C_k becomes negative, and there is energy conserved from PPE to KE, which increases the local Hadley circulation intensity as well. Thus, the overall effects make the Hadley circulations increase significantly in the central–western Pacific. On the other hand, there are anomalous northerly winds in the Northern Hemisphere and southerly winds in the Southern Hemisphere to the east of the PPEa center, which indicates that there is anomalous descending air in the eastern Pacific. As warm air descends, C_k is positive, which is opposite of the central–western Pacific. In the Gill model, the downward wind in the east is weak, and the energy conversion is not quite significant; thus, the Hadley circulation signals are weaker in the east than in the central–western Pacific. The situation reverses in the decaying phase of La Niña.

b. *Effect of Hadley circulation on ENSO phase transition*

The regional Hadley circulation change can have an influence on the surface zonal winds, which is crucial in ENSO dynamics. The lead–lag correlations between the western Pacific surface zonal wind U and the in Fig. 13a show that the westerly wind bursts in the western Pacific about four months before El Niño matures, and easterly winds increase in the summer of the next year. Comparing the results in Fig. 13c, U lags NWHCI similar to the Niño-3.4 index shown in Fig. 13a, but the correlations are more significant. The surface easterly wind peaks in the western Pacific four months after the central–western Hadley circulation intensifies. When calculating the partial correlation between U and the Niño-3.4 index by removing the NWHCI signal (Fig. 13b), the positive correlation decreases, while the negative correlations remain the same but are still not significant. The weakened partial correlations indicate that the central–western Pacific Hadley circulations serve as a bridge in linking the central–eastern Pacific SST and the central–western Pacific surface zonal winds. On the other hand, when removing the Niño-3.4 signal, the partial correlations between U and NWHCI increase significantly (Fig. 13d). This demonstrates that the surface zonal winds in the western Pacific have a more direct link with the local Hadley circulation than with SST. The results in Figs. 13e,f illustrate that there is strong equatorial KE convergence in the western Pacific when the Hadley circulations strengthen over the central–western Pacific in El Niño. This surface KE convergence

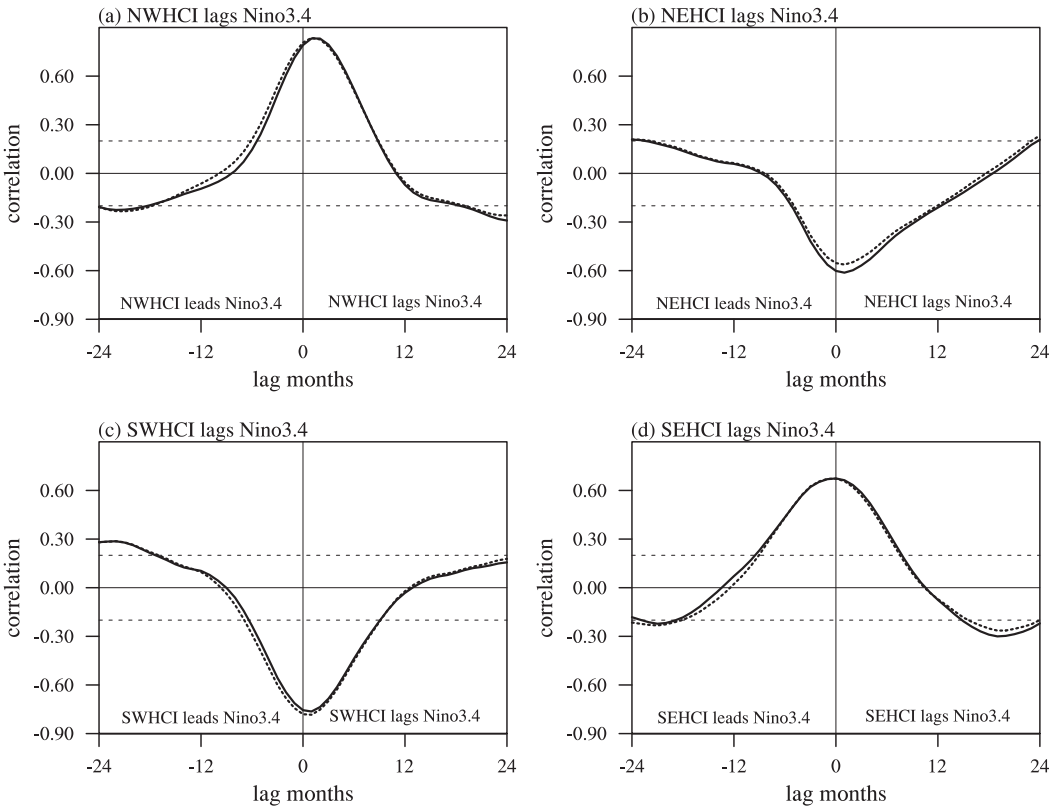

FIG. 12. Lead–lag correlations between the Niño-3.4 index and HCI for (a) NWHCI, (b) NEHCI, (c) SWHCI, and (d) SEHCI. Solid lines are based on NCEP-2 data, and dotted lines are based on ERA-Interim data. Positive values indicate that HCI lags the Niño-3.4 index, and thin dashed lines are 95% confidence levels.

may explain how the strengthened Hadley circulations increase the easterlies after El Niño matures, and vice versa for La Niña.

Based on the above analysis, it is noticed that the central–western Pacific Hadley circulations can change the western Pacific surface zonal winds through the KE convergence or divergence after ENSO matures. Since the western Pacific surface zonal wind bursts are a triggering mechanism of El Niño or La Niña, and the Hadley circulation effect on the zonal wind bursts occurs drastically in the boreal spring, this process may serve as a negative feedback to reverse the ENSO phase. To explain this negative feedback lucidly, a schematic diagram is illustrated in Fig. 14.

Suppose a typical El Niño event develops in the tropical Pacific, reaching its mature phase in December. The atmospheric diabatic heating increases and reaches a maximum in February of the next year. The latent heat release in the midtroposphere leads to an atmospheric PPE increase in the form of the Gill model response, with two anticyclones forming at the upper troposphere over the central Pacific. The anticyclonic circulations in the upper troposphere increase the poleward meridional velocities to the west of the PPEa center, which strengthen the rising motion of the air. Thus, more energy is converted to atmospheric KE, and Hadley circulations strengthen in the central–western equatorial Pacific. Meanwhile, the condition is opposite over the eastern Pacific where the vertical velocities are quite weak, and the local Hadley circulations weaken. As a result, the central–western Pacific Hadley circulation converges more KE to the equatorial zone and increases surface wind power therein, while the weakened eastern Hadley cells result in less KE convergence at the equator. Thus, the easterly wind bursts occur in the western equatorial Pacific region. With easterly wind bursts in the western Pacific, the positive Bjerknes feedback starts to dominate the air–sea interactions, the equatorial current intensifies, the thermocline slope gets steeper, and it is possible for a La Niña event to develop.

On the other hand, after La Niña matures in December, the diabatic heating reaches a minimum in the late boreal winter of the next year, leading to two minimum PPEa centers with cyclonic circulation symmetric

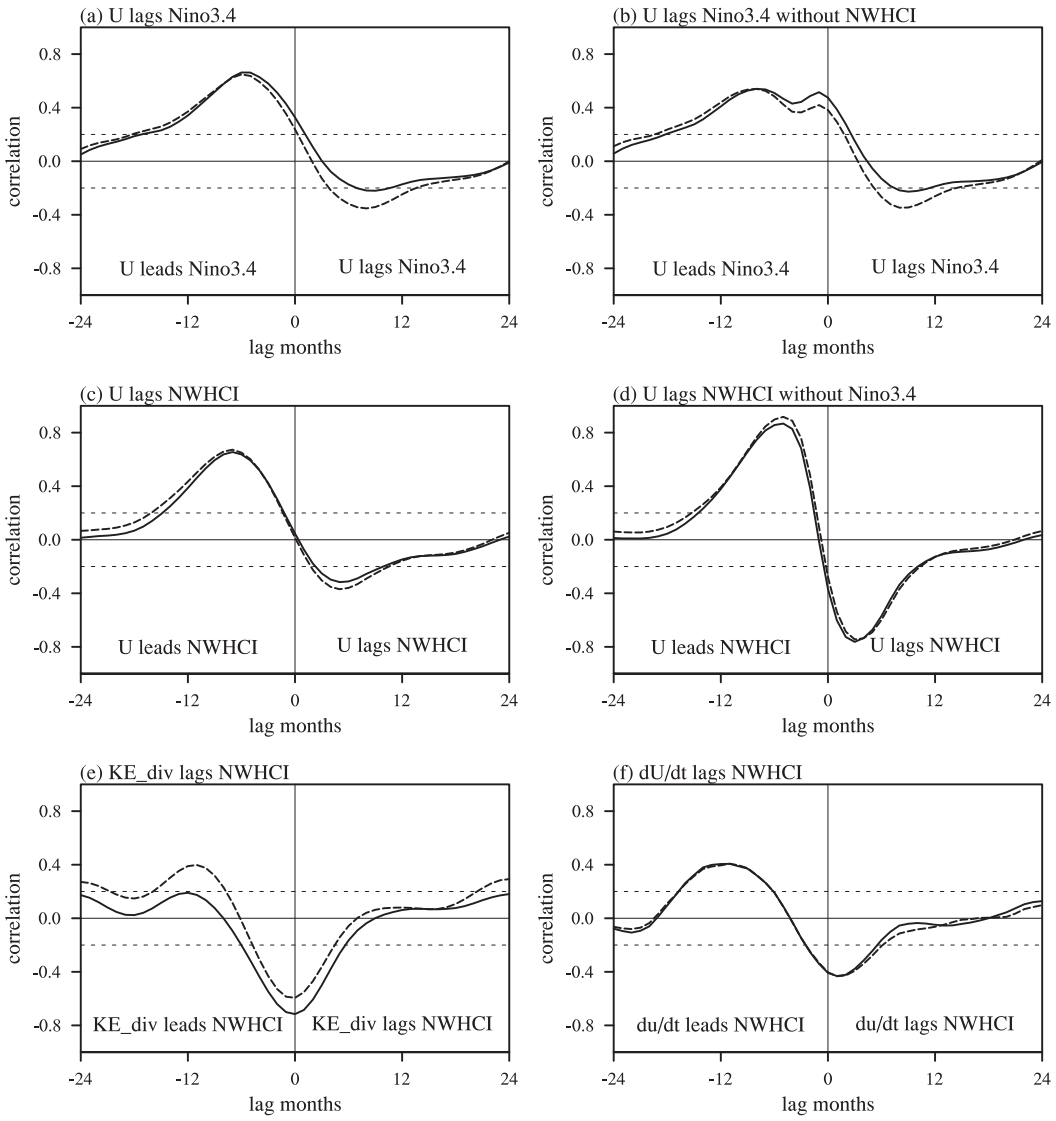

FIG. 13. (a) Lead–lag correlations between *U* and the Niño-3.4 index, where *U* is the areal mean of western Pacific surface zonal winds, and positive values indicate *U* lags the Niño-3.4 index. (b) As in (a), but removing the NWHCI signal. (c) Lead–lag correlations between *U* and NWHCI. (d) As in (c), but removing the Niño-3.4 index. (e) Lead–lag correlations between KE_div and NWHCI, where KE_div is the area mean of surface KE divergence over the western Pacific. (f) Lead–lag correlations between dU/dt and NWHCI, where dU/dt is the time derivative of *U* in the western Pacific. The solid lines are calculated with NCEP-2 data, and the dashed lines are based on ERA-Interim data.

about the equator in the upper troposphere. During this period, the tropical Pacific atmosphere has much less energy than normal, and less energy is converted to atmospheric KE in the western Pacific. Thus, the Hadley circulations weaken in the west but strengthen in the east. As a result, the weakened central–western Pacific Hadley circulations converge less KE and decrease wind speed along the western Pacific equatorial zone. Consequently, anomalous westerly wind bursts are likely to occur in the western Pacific. This then may lead to another El Niño event through the positive air–sea feedback.

6. Summary

By comparing two reanalysis datasets, this study investigated variations in tropical Pacific atmospheric energetics and their impact on the regional Hadley circulations and proposed a possible negative feedback in the atmosphere during an ENSO cycle. The atmospheric

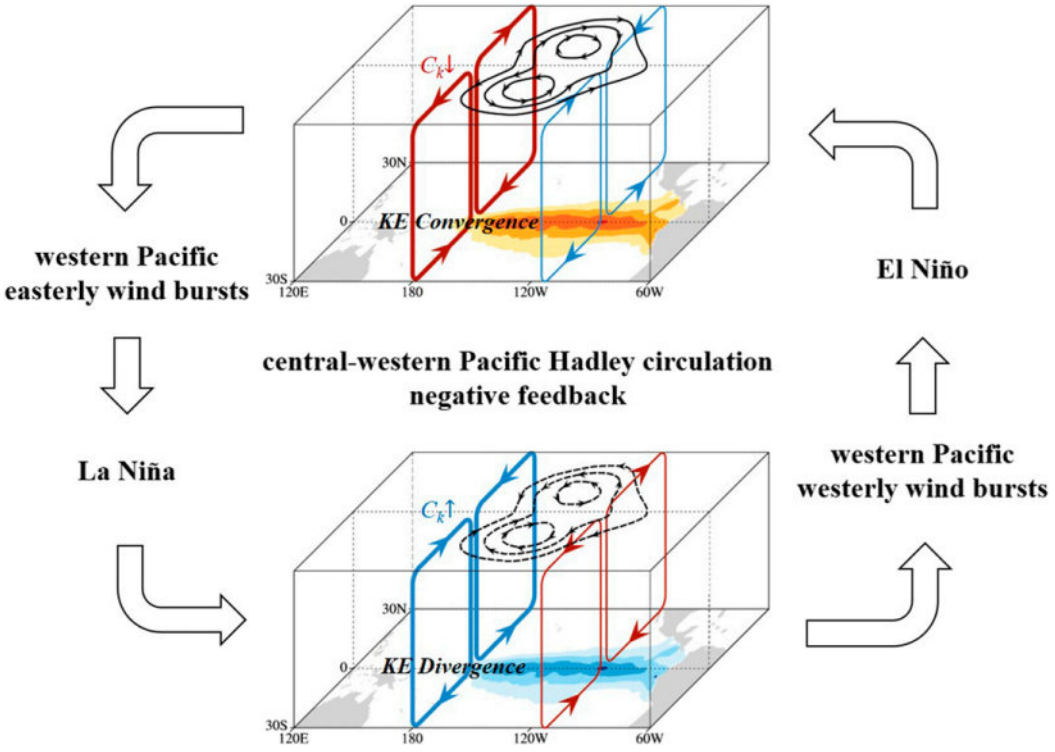

FIG. 14. Schematic diagram of tropical Pacific atmospheric energy changes and Hadley circulation negative feedback in an ENSO cycle. Color shading indicates composite SST anomalies: red–yellow shading represents anomalously high SST in El Niño and blue shading represents anomalously low SST in La Niña. Red circulation lines represent intensified Hadley circulation, blue circulation lines represent weakened Hadley circulation, and line thickness indicates the intensity of the Hadley circulation response. Black solid streamlines show the anomalously high PPE at the upper troposphere in El Niño, and black dashed streamlines show the anomalously low PPE at the upper troposphere in La Niña.

PPE has been used as a diagnostic tool to study the local atmospheric available energetics in this study, since the PPE theory redefines the minimum reference state and extends the classic APE to a regional scale (Li and Gao 2006). Combining this with the ENSO oceanic energetics (Goddard and Philander 2000; Brown and Fedorov 2010), a complete energy cycle of the tropical Pacific air–sea system can be pictured in Fig. 15. From an energetic view, one major issue is explored: how the anomalous SST in the central–eastern Pacific influences the surface winds in the western Pacific through the atmospheric energy transport and conversion during a typical ENSO cycle. Three main processes are involved:

1) SST anomalies influence atmospheric PPE through diabatic heating. There is increased heat transported from the ocean to the air in El Niño and decreased heat release in La Niña. Two heating processes coexist in an ENSO event: At the bottom of the troposphere, PPEa is consistent with SSTa both temporally and spatially, which is linked to sensible heating; in the mid- and upper troposphere, PPEa shows two centers symmetrical about the equator in the central Pacific and delays SSTa by 2 or 3 months, which results from the latent heat release. Since the latent heat release is much larger than the sensible heating, PPE has its maximum or minimum centers mainly in the midtroposphere.
2) The energy conversion between atmospheric PPE and KE. The energy conversion during ENSO is the most intense over the central–western Pacific in the boreal late winter or spring. In El Niño, more energy is converted to atmospheric KE to increase the Hadley circulation over the central–western Pacific, while the atmosphere gains less KE and Hadley circulations weaken over the eastern Pacific. The condition is opposite during La Niña.
3) Hadley circulations in the central–western Pacific change the surface zonal winds in the western Pacific. In El Niño, the central–western Pacific Hadley circulations intensify and converge KE to the equatorial western Pacific, increasing the easterlies therein. In contrast, during La Niña, the central–western Pacific Hadley circulations weaken and decrease the local surface zonal winds.

These three processes depict how the atmospheric energetics respond to the ocean heating and provide a

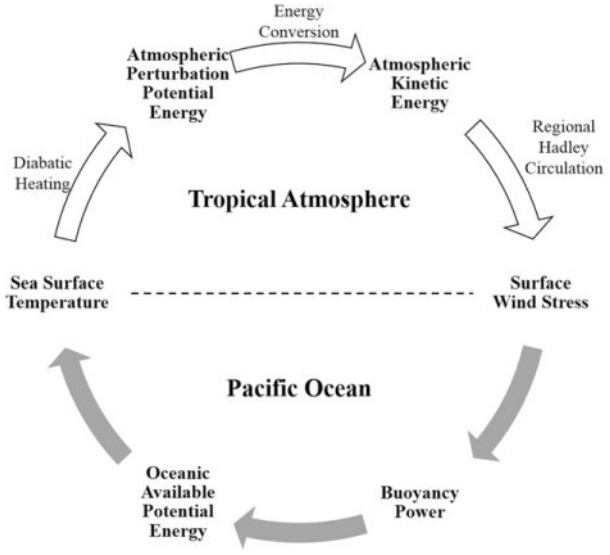

FIG. 15. A schematic diagram of energy cycle in the tropical Pacific air–sea system during ENSO events. The oceanic part is from Brown and Fedorov (2010), and the atmospheric part is based on this study.

possible explanation of how the central–eastern Pacific SSTa can influence the surface zonal winds in the western Pacific and why westerly or easterly wind bursts mainly start to develop in the western Pacific. From Fig. 15, as the surface winds change in the western Pacific, they modify the ocean's energy distribution, which in turn influences the sea surface temperature. Thus, the modified energy distribution forms a cycle in the ocean and atmosphere of the tropical Pacific region, demonstrating the strong air–sea interaction during ENSO events. In fact, the essence of the air–sea interaction is the energy exchange between the ocean and the atmosphere. Focusing on the energetics makes the air–sea coupling process physically understood.

However, it is also noted that ENSO events are full of diversity and complexity. Furthermore, we have compared the PPE response in strong and weak El Niño events and found the PPE signal is significant even at the top of the troposphere in strong El Niño events. Also, the PPEs in eastern-Pacific (EP) and central-Pacific (CP) El Niño events (Kao and Yu 2009) are also compared, which shows that the PPE center is shifted westward in the CP El Niño, where the maximum SSTa lies in the central Pacific. The results demonstrate that the atmospheric PPE variations are closely associated with the intensity and location of SSTa in ENSO events. Therefore, more detailed research on the PPE response for different types of ENSO events and how PPE in the tropical Pacific interacts with the atmospheric energy at midlatitudes and over other ocean basins are essential in a further stage.

Acknowledgments. This work was supported by the National Natural Science Foundation of China (41530424), MOST Key Project (2016YFA0601801), and the SOA International Cooperation Program on Global Change and Air–Sea Interactions (GASI-IPOVAI-03).

APPENDIX A

Atmospheric PPE

The total potential energy (TPE) of an air column per unit area is

$$\mathrm{TPE} = \int_{z_s}^{\infty} \rho(gz + c_v T)\, dz = \frac{1}{\gamma_d} \int_0^{p_s} T\, dp + z_s p_s, \qquad \text{(A1)}$$

where ρ is air density; g is the gravitational acceleration; z_s is surface topography; c_v is the specific heat at constant volume; $\gamma_d = g/c_p$, where c_p is the specific heat at constant pressure; T is temperature; p is pressure; and p_s is surface pressure. Considering an adiabatic process, Eq. (A1) can be written in an isentropic coordinate system:

$$\begin{aligned}\mathrm{TPE} &= \frac{1}{\gamma_d} \int_0^{p_s} \theta (p/p_{00})^{\kappa}\, dp + z_s p_s \\ &= \frac{1}{(1+\kappa)\gamma_d p_{00}^{\kappa}} \int_{\theta_s}^{\theta_t} p^{1+\kappa}\, d\theta \\ &\quad + \frac{1}{(1+\kappa)\gamma_d p_{00}^{\kappa}} \theta_s p_s^{1+\kappa} + z_s p_s, \end{aligned} \qquad \text{(A2)}$$

where θ is potential temperature and θ_s and θ_t are potential temperatures at the surface and the tropopause, respectively; $\kappa = R/c_p$, where R is the gas constant for dry air; and p_{00} is the reference pressure (usually 1000 hPa). In Eq. (A2), the TPE of an air column contains two parts: the first term on the left is the atmospheric energy part; the second and third terms combined are associated with the surface conditions.

Li and Gao (2006) defined PPE as the atmospheric TPE difference between the actual state and the reference state via adiabatic redistribution. Lorenz (1955) defined the reference state as the minimum TPE when stratification is horizontal and statically stable. Gao et al. (2006) found this minimum

TPE state is unreachable physically. They proposed a conditional minimum TPE state (here we add an overbar to the physical variables to denote this state) and demonstrated that $\overline{\theta}_s = \theta_s$ and $\overline{\theta}_t = \theta_t$ during a dry adiabatic process in the atmosphere; thus,

$$\mathrm{TPE}_{\mathrm{actual}} - \mathrm{TPE}_{\mathrm{ref}} = \mathrm{PPE} + \mathrm{SPPE}, \tag{A3}$$

$$\mathrm{PPE} = \frac{1}{(1+\kappa)\gamma_d p_{00}^{\kappa}} \int_{\theta_s}^{\theta_t} (p^{1+\kappa} - \overline{p}^{1+\kappa})\, d\theta, \quad \text{and} \tag{A4}$$

$$\mathrm{SPPE} = \frac{1}{(1+\kappa)\gamma_d p_{00}^{\kappa}} (\theta_s p_s^{1+\kappa} - \overline{\theta}_s \overline{p}_s^{1+\kappa}) + (z_s p_s - \overline{z}_s \overline{p}_s). \tag{A5}$$

Here, PPE is the atmospheric perturbation potential energy, and SPPE is the surface perturbation potential energy that is related to the surface topographic conditions. If we let $p = \overline{p} + p'$, PPE can be written in the following form:

$$\begin{aligned}
\mathrm{PPE} &= \frac{1}{(1+\kappa)\gamma_d p_{00}^{\kappa}} \int_{\theta_s}^{\theta_t} [(\overline{p} + p')^{1+\kappa} - \overline{p}^{1+\kappa}]\, d\theta \\
&= \frac{1}{(1+\kappa)\gamma_d p_{00}^{\kappa}} \int_{\theta_s}^{\theta_t} (1+\kappa)\overline{p}^{1+\kappa} \left[\frac{p'}{\overline{p}} + \frac{\kappa}{2}\left(\frac{p'}{\overline{p}}\right)^2 + \frac{\kappa(\kappa-1)}{3!}\left(\frac{p'}{\overline{p}}\right)^3 + \cdots \right] d\theta \\
&= \frac{1}{\gamma_d p_{00}^{\kappa}} \int_{\theta_s}^{\theta_t} \overline{p}^{1+\kappa} \left[\frac{p'}{\overline{p}} + \frac{\kappa}{2}\left(\frac{p'}{\overline{p}}\right)^2 + \frac{\kappa(\kappa-1)}{3!}\left(\frac{p'}{\overline{p}}\right)^3 + \cdots \right] d\theta.
\end{aligned} \tag{A6}$$

The perturbation pressure p' on an isentropic surface and the perturbation potential temperature θ' on an isobaric surface have the following relation: $p'(\theta) \approx -\theta' \partial\overline{p}/\partial\theta$ (Lorenz 1955). PPE in isobaric coordinates can be written as follows:

$$\mathrm{PPE} = \sum_{i=1}^{\infty} \frac{\prod_{j=0}^{i-1}(1+\kappa-j)}{i!\gamma_d(1+\kappa)p_{00}^{\kappa}} \int_0^{p_s} p^{(1+\kappa-i)} \theta'^{i} \left(-\frac{\partial\overline{\theta}}{\partial p}\right)^{-i+1} dp. \tag{A7}$$

Using the relation $\theta' = T'(p_{00}/p)^{\kappa}$, PPE can also be written as follows:

$$\mathrm{PPE} = \sum_{i=1}^{\infty} \frac{p_{00}^{(i-1)\kappa} \prod_{j=0}^{i-1}(1+\kappa-j)}{i!\gamma_d(1+\kappa)} \int_0^{p_s} \frac{T'^{i}}{p^{(i-1)(1+\kappa)}} \left(-\frac{\partial\overline{\theta}}{\partial p}\right)^{-i+1} dp, \tag{A8}$$

where the ith term at right denotes the ith-moment term of PPE. According to Li and Gao (2006), in a regional scale, the first-moment PPE_1 is an order of magnitude larger than PPE_2, and, on a global average, PPE_1 diminishes, while PPE_2 is the major term; the other higher-moment terms are much smaller compared to PPE_1 and PPE_2; thus, PPE can be approximated as follows:

$$\begin{aligned}
\mathrm{PPE} &\approx \mathrm{PPE}_1 + \mathrm{PPE}_2 \\
&= \frac{1}{\gamma_d} \int_0^{p_s} T'\, dp + \frac{\kappa p_{00}^{\kappa}}{2\gamma_d} \int_0^{p_s} \frac{T'^2}{p^{1+\kappa}} \left(-\frac{\partial\overline{\theta}}{\partial p}\right)^{-1} dp.
\end{aligned} \tag{A9}$$

APPENDIX B

The Governing Equation of PPE_1

The atmosphere thermodynamic equation is

$$c_p \frac{dT}{dt} - \alpha\omega = Q, \tag{B1}$$

where $\omega = dp/dt$, and Q is the diabatic heating rate to the atmosphere. Combing the continuity equation, Eq. (B1) can be written as

$$\frac{\partial T}{\partial t} - \nabla_h \cdot (\mathbf{V}_h T) + \frac{\partial \omega T}{\partial p} = \frac{1}{c_p}(\alpha\omega + Q). \tag{B2}$$

When writing Eq. (B2) in the global reference state, $\nabla_h \cdot (\mathbf{V}_h T)$ diminishes, and it becomes

$$\frac{\partial \overline{T}}{\partial t} + \frac{\partial \overline{\omega T}}{\partial p} = \frac{1}{c_p}(\overline{\alpha\omega} + \overline{Q}). \tag{B3}$$

Similarly, we define the local temperature deviation to the reference state as $T' = T - \overline{T}$ and get the equation of T' using Eq. (B2) minus Eq. (B3):

$$\frac{\partial T'}{\partial t} = -\nabla \cdot (\mathbf{V}_h T) - \frac{\partial}{\partial p}(\omega T - \overline{\omega T}) + \frac{1}{c_p}(\omega\alpha - \overline{\omega\alpha}) + \frac{1}{c_p}(Q - \overline{Q}). \quad \text{(B4)}$$

When integrating Eq. (B4) from the surface to the top of the atmosphere, $\int_0^{p_s} \partial/\partial p(\omega T - \overline{\omega T})\, dp$ diminishes, and it becomes

$$\int_0^{p_s} \frac{\partial T'}{\partial t}\, dp = \frac{1}{c_p}\int_0^{p_s} (\omega\alpha - \overline{\omega\alpha})\, dp + \frac{1}{c_p}\int_0^{p_s} (Q - \overline{Q})\, dp - \int_0^{p_s} \nabla \cdot (\mathbf{V}_h T)\, dp. \quad \text{(B5)}$$

Since $\mathrm{PPE}_1 = \gamma_d^{-1}\int_0^{p_s} T'\, dp$, Eq. (B5) can be transformed into the governing equation of PPE_1:

$$\frac{\partial \mathrm{PPE}_1}{\partial t} = \underbrace{\frac{1}{g}\int_0^{p_s} (\omega\alpha - \overline{\omega\alpha})\, dp}_{C_k} + \underbrace{\frac{1}{g}\int_0^{p_s} (Q - \overline{Q})\, dp}_{G} - \underbrace{\int_0^{p_s} \nabla \cdot (\mathbf{V}_h \mathrm{PPE}_1)\, dp}_{\mathrm{HBF}}. \quad \text{(B6)}$$

From Eq. (B6), the atmospheric PPE_1 is controlled with three terms: the energy conversion with KE C_k, the diabatic heating rate G, and the horizontal boundary fluxes of PPE_1 HBF.

REFERENCES

Angell, J. K., 1981: Comparison of variations in atmospheric quantities with sea surface temperature variations in the equatorial eastern Pacific. *Mon. Wea. Rev.*, **109**, 230–243, doi:10.1175/1520-0493(1981)109<0230:COVIAQ>2.0.CO;2.

Belamari, S., J. L. Redelsperger, and M. Pontaud, 2003: Dynamic role of a westerly wind burst in triggering an equatorial Pacific warm event. *J. Climate*, **16**, 1869–1890, doi:10.1175/1520-0442(2003)016<1869:DROAWW>2.0.CO;2.

Bjerknes, J., 1969: Atmospheric teleconnections from the equatorial Pacific. *Mon. Wea. Rev.*, **97**, 163–172, doi:10.1175/1520-0493(1969)097<0163:ATFTEP>2.3.CO;2.

Boulanger, J. P., and Coauthors, 2001: Role of non-linear oceanic processes in the response to westerly wind events: New implications for the 1997 El Niño onset. *Geophys. Res. Lett.*, **28**, 1603–1606, doi:10.1029/2000GL012364.

Brown, J. N., and A. V. Fedorov, 2008: Mean energy balance in the tropical Pacific Ocean. *J. Mar. Res.*, **66**, 1–23, doi:10.1357/002224008784815757.

——, and ——, 2010: How much energy is transferred from the winds to the thermocline on ENSO time scales? *J. Climate*, **23**, 1563–1580, doi:10.1175/2009JCLI2914.1.

Chen, D., and Coauthors, 2015: Strong influence of westerly wind bursts on El Niño diversity. *Nat. Geosci.*, **8**, 339–345, doi:10.1038/ngeo2399.

Dee, D. P., and Coauthors, 2011: The ERA-Interim reanalysis: Configuration and performance of the data assimilation system. *Quart. J. Roy. Meteor. Soc.*, **137**, 553–597, doi:10.1002/qj.828.

Edmon, H. J., Jr., 1978: A reexamination of limited-area available potential energy budget equations. *J. Atmos. Sci.*, **35**, 1655–1659, doi:10.1175/1520-0469(1978)035<1655:AROLAA>2.0.CO;2.

Eisenman, I., L. Yu, and E. Tziperman, 2005: Westerly wind bursts: ENSO's tail rather than the dog? *J. Climate*, **18**, 5224–5238, doi:10.1175/JCLI3588.1.

Fedorov, A. V., 2007: Net energy dissipation rates in the tropical ocean and ENSO dynamics. *J. Climate*, **20**, 1108–1117, doi:10.1175/JCLI4024.1.

——, S. L. Harper, S. G. Philander, B. Winter, and A. Wittenberg, 2003: How predictable is El Niño? *Bull. Amer. Meteor. Soc.*, **84**, 911–919, doi:10.1175/BAMS-84-7-911.

Gao, L., and J. P. Li, 2012: Relationship and mechanism between perturbation potential energy and atmospheric general circulation anomalies. *Chin. J. Geophys.*, **55**, 359–374, doi:10.1002/cjg2.1730.

——, and ——, 2013: Impacts and mechanism of diabatic heating on atmospheric perturbation potential energy. *Chin. J. Geophys.*, **56**, 3255–3269, doi:10.6038/cjg20131004.

——, ——, and H. L. Ren, 2006: Some characteristics of the atmosphere during an adiabatic process. *Prog. Nat. Sci.*, **16**, 644–648, doi:10.1080/10020070612330047.

Giese, B. S., and D. E. Harrison, 1990: Aspects of the Kelvin wave response to episodic wind forcing. *J. Geophys. Res.*, **95**, 7289–7312, doi:10.1029/JC095iC05p07289.

——, and ——, 1991: Eastern equatorial Pacific response to three composite westerly wind types. *J. Geophys. Res.*, **96**, 3239–3248, doi:10.1029/90JC01861.

Gill, A. E., 1980: Some simple solutions for heat-induced tropical circulation. *Quart. J. Roy. Meteor. Soc.*, **106**, 447–462, doi:10.1002/qj.49710644905.

Goddard, L., and S. G. Philander, 2000: The energetics of El Niño and La Niña. *J. Climate*, **13**, 1496–1516, doi:10.1175/1520-0442(2000)013<1496:TEOENO>2.0.CO;2.

Godfrey, J. S., 1975: On ocean spindown I: A linear experiment. *J. Phys. Oceanogr.*, **5**, 399–409, doi:10.1175/1520-0485(1975)005<0399:OOSIAL>2.0.CO;2.

Harrison, D. E., and A. M. Chiodi, 2009: Pre-and post-1997/98 westerly wind events and equatorial Pacific cold tongue warming. *J. Climate*, **22**, 568–581, doi:10.1175/2008JCLI2270.1.

Hu, S., and A. V. Fedorov, 2016: Exceptionally strong easterly wind burst stalling El Niño of 2014. *Proc. Natl. Acad. Sci. USA*, **113**, 2005–2010, doi:10.1073/pnas.1514182113.

——, ——, M. Lengaigne, and E. Guilyardi, 2014: The impact of westerly wind bursts on the diversity and predictability of El Niño events: An ocean energetics perspective. *Geophys. Res. Lett.*, **41**, 4654–4663, doi:10.1002/2014GL059573.

Jin, F. F., 1997a: An equatorial ocean recharge paradigm for ENSO. Part I: Conceptual model. *J. Atmos. Sci.*, **54**, 811–829, doi:10.1175/1520-0469(1997)054<0811:AEORPF>2.0.CO;2.

——, 1997b: An equatorial ocean recharge paradigm for ENSO. Part II: A stripped-down coupled model. *J. Atmos. Sci.*, **54**, 830–847, doi:10.1175/1520-0469(1997)054<0830:AEORPF>2.0.CO;2.

Johnson, D. R., 1970: The available potential energy of storms. *J. Atmos. Sci.*, **27**, 727–741, doi:10.1175/1520-0469(1970)027<0727:TAPEOS>2.0.CO;2.

Kao, H. Y., and J. Y. Yu, 2009: Contrasting eastern-Pacific and central-Pacific types of ENSO. *J. Climate*, **22**, 615–632, doi:10.1175/2008JCLI2309.1.

Kanamitsu, M., W. Ebisuzaki, J. Woollen, S. Yang, J. Hnilo, M. Fiorino, and G. Potter, 2002: NCEP–DOE AMIP-II Reanalysis (R-2). *Bull. Amer. Meteor. Soc.*, **83**, 1631–1643, doi:10.1175/BAMS-83-11-1631.

Kumar, A., and M. P. Hoerling, 2003: The nature and causes for the delayed atmospheric response to El Niño. *J. Climate*, **16**, 1391–1403, doi:10.1175/1520-0442-16.9.1391.

Lengaigne, M., E. Guilyardi, J.-P. Boulanger, C. Menkes, P. Delecluse, P. Inness, J. Cole, and J. Slingo, 2004: Triggering of El Niño by westerly wind events in a coupled general circulation model. *Climate Dyn.*, **23**, 601–620, doi:10.1007/s00382-004-0457-2.

Li, J. P., and L. Gao, 2006: Theory on perturbation potential energy and its applications—Concept, expression and spatiotemporal structures of perturbation potential energy (in Chinese). *Chin. J. Atmos. Sci.*, **30**, 834–848.

——, Z. Sen, L. Yanjie, W. Lei, and S. Cheng, 2016: On the role of perturbation potential energy in variability of the East Asian summer monsoon: Current status and prospects. *Adv. Earth Sci.*, **31**, 115–125, doi:10.11867/j.issn.1001-8166.2016.02.0115.

Li, L., M. T. Chahine, X. Jiang, and Y. L. Yung, 2011: The mechanical energies of the global atmosphere in El Niño and La Niña years. *J. Atmos. Sci.*, **68**, 3072–3078, doi:10.1175/JAS-D-11-072.1.

Lopez, H., B. P. Kirtman, E. Tziperman, and G. Gebbie, 2013: Impact of interactive westerly wind bursts on CCSM3. *Dyn. Atmos. Oceans*, **59**, 24–51, doi:10.1016/j.dynatmoce.2012.11.001.

Lorenz, E. N., 1955: Available potential energy and the maintenance of the general circulation. *Tellus*, **7**, 157–167, doi:10.3402/tellusa.v7i2.8796.

Margules, M., 1910: Uber die energie der stiirme (On the energy of storms). *Smithson. Misc. Collect.*, **51**, 533–595.

McCreary, J. P., 1976: Eastern tropical ocean response to changing wind systems: With application to El Niño. *J. Phys. Oceanogr.*, **6**, 632–645, doi:10.1175/1520-0485(1976)006<0632:ETORTC>2.0.CO;2.

McPhaden, M. J., and X. Yu, 1999: Equatorial waves and the 1997–98 El Niño. *Geophys. Res. Lett.*, **26**, 2961–2964, doi:10.1029/1999GL004901.

——, H. P. Freitag, S. P. Hayes, and B. A. Taft, 1988: The response of the equatorial Pacific Ocean to westerly wind burst in May 1986. *J. Geophys. Res.*, **93**, 10 589–10 603, doi:10.1029/JC093iC09p10589.

Moore, D. W., and S. G. H. Philander, 1977: Modeling of the tropical oceanic circulation. *Marine Modeling*, E. D. Goldberg et al., Eds., *The Sea—Ideas and Observations on Progress in the Study of the Seas.*, Vol. 6, Wiley, 319–361.

Neelin, J. D., D. S. Battisti, A. C. Hirst, F. F. Jin, Y. Wakata, T. Yamagata, and S. E. Zebiak, 1998: ENSO theory. *J. Geophys. Res.*, **103**, 14 261–14 290, doi:10.1029/97JC03424.

Oort, A. H., 1964: On estimates of the atmospheric energy cycle. *Mon. Wea. Rev.*, **92**, 483–493, doi:10.1175/1520-0493(1964)092<0483:OEOTAE>2.3.CO;2.

——, 1971: The observed annual cycle in the meridional transport of atmospheric energy. *J. Atmos. Sci.*, **28**, 325–339, doi:10.1175/1520-0469(1971)028<0325:TOACIT>2.0.CO;2.

——, S. C. Ascher, S. Levitus, and J. P. Peixóto, 1989: New estimates of the available potential energy in the world ocean. *J. Geophys. Res.*, **94**, 3187–3200, doi:10.1029/JC094iC03p03187.

Pan, Y. H., and A. H. Oort, 1983: Global climate variations connected with sea surface temperature anomalies in the eastern equatorial Pacific Ocean for the 1958–73 period. *Mon. Wea. Rev.*, **111**, 1244–1258, doi:10.1175/1520-0493(1983)111<1244:GCVCWS>2.0.CO;2.

Peixóto, J. P., and A. H. Oort, 1974: The annual distribution of atmospheric energy on a planetary scale. *J. Geophys. Res.*, **79**, 2149–2159, doi:10.1029/JC079i015p02149.

Philander, S. G., and A. Fedorov, 2003: Is El Niño sporadic or cyclic? *Annu. Rev. Earth Planet. Sci.*, **31**, 579–594, doi:10.1146/annurev.earth.31.100901.141255.

Picaut, J., F. Masia, and Y. Du Penhoat, 1997: An advective-reflective conceptual model for the oscillatory nature of the ENSO. *Science*, **277**, 663–666, doi:10.1126/science.277.5326.663.

Rayner, N. A., D. E. Parker, E. B. Horton, C. K. Folland, L. V. Alexander, D. P. Rowell, E. C. Kent, and A. Kaplan, 2003: Global analyses of sea surface temperature, sea ice, and night marine air temperature since the late nineteenth century. *J. Geophys. Res.*, **108**, 4407, doi:10.1029/2002JD002670.

Reid, G. C., K. S. Gage, and J. R. McAfee, 1989: The thermal response of the tropical atmosphere to variations in equatorial Pacific sea surface temperature. *J. Geophys. Res.*, **94**, 14 705–14 716, doi:10.1029/JD094iD12p14705.

Schumacher, C., R. A. Houze Jr., and I. Kraucunas, 2004: The tropical dynamical response to latent heating estimates derived from the TRMM precipitation radar. *J. Atmos. Sci.*, **61**, 1341–1358, doi:10.1175/1520-0469(2004)061<1341:TTDRTL>2.0.CO;2.

Smith, P. J., 1969: On the contribution of a limited region to the global energy budget. *Tellus*, **21**, 202–207, doi:10.1111/j.2153-3490.1969.tb00432.x.

——, D. G. Vincent, and H. J. Edmon, 1977: The time dependence of reference pressure in limited region available potential energy budget equations. *Tellus*, **29**, 476–480, doi:10.1111/j.2153-3490.1977.tb00759.x.

Su, H., J. D. Neelin, and J. E. Meyerson, 2005: Mechanisms for lagged atmospheric response to ENSO SST forcing. *J. Climate*, **18**, 4195–4215, doi:10.1175/JCLI3514.1.

Suarez, M. J., and P. S. Schopf, 1988: A delayed action oscillator for ENSO. *J. Atmos. Sci.*, **45**, 3283–3287, doi:10.1175/1520-0469(1988)045<3283:ADAOFE>2.0.CO;2.

Tao, W. K., and Coauthors, 2001: Retrieved vertical profiles of latent heat release using TRMM rainfall products for February 1998. *J. Appl. Meteor.*, **40**, 957–982, doi:10.1175/1520-0450(2001)040<0957:RVPOLH>2.0.CO;2.

Vecchi, G. A., and D. E. Harrison, 2000: Tropical Pacific sea surface temperature anomalies, El Niño, and equatorial westerly wind events. *J. Climate*, **13**, 1814–1830, doi:10.1175/1520-0442(2000)013<1814:TPSSTA>2.0.CO;2.

Wang, L., J. P. Li, and Y. Guo, 2012: Governing equations of atmospheric layer perturbation potential energy and its applications—Energy budget of the South China Sea summer monsoon activity. *Chin. J. Atmos. Sci.*, **36**, 769–783.

——, J. Li, Z. Wang, Y. Li, and F. Zheng, 2015: The oscillation of the perturbation potential energy between the extra-tropics and tropics in boreal winter. *Atmos. Sci. Lett.*, **16**, 119–126, doi:10.1002/asl2.532.

Weisberg, R. H., and C. A. Wang, 1997: Western Pacific oscillator paradigm for the El Niño–Southern Oscillation. *Geophys. Res. Lett.*, **24**, 779–782, doi:10.1029/97GL00689.

Yu, L., R. A. Weller, and W. T. Liu, 2003: Case analysis of a role of ENSO in regulating the generation of westerly wind bursts in the western equatorial Pacific. *J. Geophys. Res.*, **108**, 3128, doi:10.1029/2002JC001498.